Impact of basin burial and exhumation on Jurassic carbonates diagenesis on both sides of a thick clay barrier (Paris Basin, NE France)

Cédric Carpentier[1], Benjamin Brigaud[2], Thomas Blaise[1], Benoît Vincent[3], Christophe Durlet[4], Philippe Boulvais[5], Maurice Pagel[2], Christian Hibsch[1], Béatrice Yven[6], Philippe Lach[1], Michel Cathelineau[1], Marie-Christine Boiron[1], Philippe Landrein[6], Stéphane Buschaert[6]

[1] GeoRessources UMR CNRS 7359, Université de Lorraine, BP 239, 54506 Vandoeuvre-lès-Nancy, France

[2] Université de Paris-Sud 11, Faculté des Sciences, Département des Sciences de la Terre, UMR CNRS-UPS IDES, 91405 - Orsay Cedex, France

[3] Cambridge Carbonates Ltd, 1 rue de Varoux, 21120 Marey-sur-Tille, France

[4] Université de Bourgogne, UMR CNRS 6282 Biogéosciences, 6 bd Gabriel, 21000 Dijon, France

[5] Géosciences, UMR 6118, Université de Rennes 1 - CNRS, Campus de Beaulieu, CS 74205, 35042 Rennes Cedex, France

[6] Andra, 1/7 rue Jean Monnet, F- 92290 Châtenay-Malabry cedex, France

Corresponding author : Cédric carpentier, G2R, Université de Lorraine, CNRS, BP 239, 54506 Vandoeuvre-lès-Nancy, France.
cedric.carpentier@univ-lorraine.fr
tel : (+33) (0)3 83 68 47 39

Abstract

Several diagenetic models have been proposed for Middle and Upper Jurassic carbonates of the eastern Paris Basin. The paragenetic sequences are compared in both aquifers to propose a diagenetic model for the Middle and Late Jurassic deposits as a whole. Petrographic (optical and cathodoluminescence microscopy), structural (fracture orientations) and geochemical ($\delta^{18}O$, $\delta^{13}C$, REE) studies were conducted to characterize diagenetic cements, with a focus on blocky calcite

cements, and their connection with fracturation events. Four generations of blocky calcite (Cal1 to Cal4) are identified. Cal1 and Cal2 are widespread in the dominantly grain-supported facies of the Middle Jurassic limestones (about 90% of the cementation), whereas they are limited in the Oxfordian because grain-supported facies are restricted to certain stratigraphic levels. Cal1 and Cal2 blocky spars precipitated during burial in a reducing environment from mixed marine-meteoric waters and/or buffered meteoric waters. The meteoric waters probably entered aquifers during the Late Cimmerian (Jurassic/Cretaceous boundary) and Late Aptian (Early Cretaceous) unconformities. The amount of Cal2 cement is thought to be linked to the intensity of burial pressure dissolution, which in turn was partly controlled by the clay content of the host rocks. Cal3 and Cal4 are associated with telogenetic fracturing phases. The succession of Cal3 and Cal4 calcite relates to the transition towards oxidizing conditions during an opening of the system to meteoric waters at higher water/rock ratios. These meteoric fluids circulated along Pyrenean, Oligocene and Alpine fractures and generated both dissolution and subsequent cementation in Oxfordian vugs in mud-supported facies and in poorly stylolitized grainstones. However, these cements filled only the residual porosity in Middle Jurassic limestones. In addition to fluorine inputs, fracturation also permitted inputs of sulphur possibly due to weathering of Triassic or Purbeckian evaporites or H_2S input during Paleogene times.

Keywords: Diagenesis, oxygen and carbon isotopes, rare earth elements, carbonate, Paris Basin, Jurassic.

1. Introduction

Several studies have been conducted in the last two decades in order to determine the origin(s) and timing of cementation of Middle and Upper Jurassic limestones in the eastern part of the Paris Basin (André et al., 2010; Granier and Staffelbach, 2009; Brigaud et al., 2009a; Buschaert et al., 2004; Javaux, 1992; Vincent et al., 2007). Both these stratigraphic intervals correspond to carbonate-dominated successions sandwiching the Callovian–Oxfordian claystones selected by the French National Agency for Radioactive Waste Management (Andra) as a site for its Underground Research Laboratory (URL) for nuclear waste disposal. Actually the porous horizons correspond to mudstones with an important microporosity while grainstones are tight. It is thus of key importance to understand

the diagenetic evolution of these aquifers in order to constrain the distribution and the evolution through space and time of reservoir properties surrounding the formation that encloses the URL.

The Middle and Upper Jurassic limestone aquifers display poor reservoir properties because of one or more extensive phases of cementation. With the exception of the early meteoric phreatic or vadose calcite spars that developed sporadically below exposure surfaces of the Middle Jurassic limestones (e.g. Javaux, 1992; Durlet and Loreau, 1996; Brigaud et al., 2009a), recent models consider that most blocky calcite cements in Middle and Upper Jurassic Limestones were generated either by meteoric water flows pre-dating the maximum burial period, or during telogenetic fracturing of the carbonates as they were exhumed. In the first case, reloads of deep aquifers during several uplifts of the basin margins in the Early Cretaceous would have been responsible for most of the cementation of both Middle and Upper Jurassic limestones (Brigaud et al., 2009a; Vincent et al., 2007), based on analogies with diagenetic models proposed for the Jurassic limestones of the Wessex-Weald Basin (Hendry, 2002). In this model, telogenetic circulations engendered substantial dissolution in the Oxfordian limestones (Vincent et al., 2007) and some cementation in the Middle Jurassic limestones (less than 10% of the total cementation; Brigaud et al., 2009a). A contrasting model argues that most cementation of the Oxfordian limestones occurred during Cenozoic telogenesis (André et al., 2010; Buschaert et al., 2004), with meteoric water flows being coeval with the formation of grabens during the Oligocene extensional tectonic regimes, or induced by fracturing during the Pyrenean and Alpine compressive stages.

This paper presents a critical reappraisal of all the published data, supplemented by a set of newly acquired results (new outcrops and drill cores, REE analyses) for Middle and Upper Jurassic limestones. The aim is to understand the evolution of the lateral and vertical hydrological pathways from Jurassic times to the present day that allowed cementation of the limestones. The main purpose is to provide a comprehensive integrated diagenetic model for both aquifers with which to better constrain the distribution of reservoir properties, which is so crucial for fluid-flow modelling.

3. Geological setting

The eastern margin of the intracratonic Paris Basin tilts westward at an inclination of about 2°. The studied outcrops of Middle and Upper Jurassic deposits are bounded by the Ardennes Massif to the north and the Burgundy High to the south (Fig. 1). Several major faults cut across the eastern margin of the basin. The Vittel, Metz and Saint-Martin de Bossenay faults are inherited from the Hercynian orogeny (Jacquin et al., 1998; Guillocheau et al., 2000). Most of these Hercynian faults were active during Mesozoic times (André et al., 2004; Carpentier et al., 2010; De Graciansky and Jacquin, 2003; Durlet et al. 1997). Faults associated with the Gondrecourt and Joinville grabens (Fig. 1) developed during the Eocene–Oligocene and are oriented NNE–SSW (André et al., 2010; Coulon and Frizon de Lamotte, 1988).

The Jurassic and Cretaceous section of the Paris Basin consists of alternating marly, sandy and carbonate formations (Fig. 2). Thick argillaceous formations (*Marnes à A. Voltzi, Marnes à Ostrea Acuminata, Argiles de la Woëvre* and *Marnes à exogyres*) alternate with carbonate formations in the Middle and Upper Jurassic succession. Several hiatuses and angular unconformities occur between the Lower Jurassic and the Upper Cretaceous (Fig. 2) (Guillocheau et al., 2000). The Mid-Cimmerian Unconformity (MCU, 175 Ma) is a hiatus with condensed deposits of iron oolites. Purbeckian deposits below the Late Cimmerian Unconformity (LCU, 145 Ma) are marked by evaporitic and dolomitic facies. The LCU and the Late Aptian Unconformity (LAU, 112 Ma) are angular unconformities between Upper Jurassic and Lower Cretaceous deposits and between Aptian and Albian deposits, respectively. The lowermost Cretaceous sandstones appear above the LCU.

The Middle Jurassic deposits consist of alternating bioclastic, oolitic, oncolitic or micritic limestones and marls (Fig. 3). The Lower Bajocian starts with marly and crinoidal limestones (*Marnes de Charannes* to the *Calcaires à entroques*). The Humphriesanum zone is characterized by alternating reefal, micritic silicified and oncolitic formations (*Calcaires à polypiers inférieurs, Oolithe Cannabine, Calcaires siliceux de l'Orne* and *Calcaires à polypiers supérieurs*) (Malartre et al., 1999; Durlet et al., 2001). The Vesulian unconformity (*sensu* Durlet and Thierry, 2000), at the Lower/Upper Bajocian boundary, is a major West European feature (Jacquin et al., 1998), which is locally expressed as an exposure surface in the eastern Paris Basin. The marly deposits of the *Marnes de Longwy* and *Marnes à Ostrea acuminata* overlie this unconformity and mark the transition from Lower to Upper

Bajocian deposits (Leroux, 1980; Mangold et al., 1994). The remainder of the Upper Bajocian and the Bathonian consists of a vertical and sometimes lateral alternating pattern of grained oolitic and oncolitic shoal deposits (*Oolithe de Jaumont*, *Oolithe miliaire inférieure*, *Oncolithe de Chaumont*, *Oolithe miliaire supérieure*, *Oolithe de Doncourt* and *Oolithe de Fréville*), marly deposits (*Marnes à Clypeus ploti* and *Marnes à Rhynchonelles*), bioclastic limestones (*Calcaires Cristallins* and *Dalle d'Etain*) and micritic lagoonal limestones (*Calcaires compacts de Neufchâteau* and *Calcaires de Chaumont*) (Brigaud et al., 2009b; Lathuilière 2008).

The interval from the Upper Callovian to the lower part of the Middle Oxfordian (Plicatilis zone) is made up of thick marl and clay deposits (*Argiles de la Woëvre* and *Marnes blanches des Eparges*) intercalated with cherty limestones and ferruginous oolites (*Terrain à Chailles* and *Oolithe ferrugineuse de Senonville*, respectively) (Megnien, 1980; Pellenard et al., 1999, 2003; Fig. 4) which overlie the Middle to Upper Callovian *Oolite Ferrugineuse* (Collin et al., 1999; Collin and Courville, 2006; Mégnien, 1980). The URL is located within the *Argiles de la Woëvre* formation.

The Middle Oxfordian deposits are characterized by alternating crinoidal, oolitic, corallian and chalky micritic limestones (Carpentier et al., 2010; Fig. 4). The peritidal deposits of the *Calcaires crayeux de Maxey* and the *Calcaires de Dainville* grade laterally southwards into the oolitic facies of the *Oolithe de Doulaincourt* (Fig. 4). To the south-west, in the Marne Valley area, peritidal limestones give way to the ammonite-rich carbonate mudstones of the *Calcaires hydrauliques*.

The Upper Oxfordian deposits consist of alternating silty marls, oolitic and bioclastic limestones, argillaceous mudstones and reefal limestones. The oolitic and bioclastic facies are laterally continuous from north to south. The Oxfordian/Kimmeridgian boundary has not been clearly identified and is located between the base of *Calcaires crayeux de Gudmont* and the top of the *Calcaires à astartes* (Lefort et al., 2011). For further information on facies distribution and the polarity of Middle and Upper Jurassic carbonate systems see Brigaud et al. in this issue.

3. Material and methods

Besides collecting and reappraising published petrographic and geochemical data, the strategy was to perform an additional comprehensive petrographic and geochemical study of the limestones of the aquifers underlying and overlying the Callovian–Oxfordian clay-rich formation of the eastern Paris Basin. Samples from grainstone/floatstone textures and calcite-filled geodes corresponding to dissolved corals entrapped in a mudstone matrix were prioritized along a SE–NW transect from Neufchâteau to the Mezières area (Fig. 1). They were collected either from quarries or from cores from the Andra wells. The EST 204, EST 205, EST 210, EST 433 and HTM 102 wells were drilled at the location or in the vicinity of the Andra URL whereas the A901 well is located in the Ardennes area (Fig. 1). Fractures were also targeted for sampling calcite infill. They were all oriented so that this study could be re-situated within the regional geodynamical time-frame described by André et al. (2010). Petrographic investigation was performed on 216 polished, half-stained, thin sections (Dickson, 1965). Cathodoluminescence (CL) was performed on the unstained half of thin sections using a CITL cold cathode instrument CL8200 Mk4 (15 kV and 500 µA). Cement volumes were quantified by building a panorama of thin sections under CL and subsequent sealing of luminescence colours with image analysis software (ImageJ). For stable isotope analyses, intergranular spars, geode infill and tension gashes were sampled by micro-drilling. In addition, when possible, calcite spar crystals from fracture infill were fragmented and collected with tweezers under the magnifying glass. The crystals were subsequently ground into a homogeneous powder in an agate mortar. Oxygen and carbon isotopes were analysed for 59 samples in the Geosciences Laboratory of Rennes University (France) (see Malfilatre et al., 2012 for analytical details). All isotopic values are reported to the V-PDB standard (Vienna-Pee Dee Belemnite). The data set is supplemented by published values for dolomite minerals (Brigaud et al., 2009a). The Rare Earth Element (REE) and major element compositions of calcite were analysed on 39 samples with LA-ICP-MS in the G2R Laboratory in Nancy (France). Calcite minerals were ablated using a 193 nm Geolas Q Plus system with an aperture-imaged Complex 103 ArF excimer laser (Microlas, Göttingen, Germany) equipped with beam homogenization optics. Ablated particulate material was analysed by an Agilent 7500c Quadrupole ICP-MS equipped with an Octopole Reaction System with an enhanced sensitivity Cs optional lens. The diameter of ablation spots is 60 µm. For REE analysis on calcite material, the internal standard was ^{40}Ca and its concentration was obtained by electron microprobe analyzer (EMPA, SCMEM Laboratory, Nancy, France). A set of fourteen REE and certain major elements (Mg, Al, Mn, Fe, Sr, and Ca) (internal

standard) were analysed for each experiment. Analytical precision was calculated for all elements analysed using standard deviation of recorded intensity and was better than ±20% for concentrations greater than 10 ppm and became greater (±50% to ±70%) for concentrations less than 10 ppm. The limit of detection (LOD) varies for each element as a function of signal intensity and was calculated for each ablation from signal intensities using the 3 σ criterion (Longerich et al., 1996). The most commonly achieved LODs were between 0.5 ppm to 1 ppm for rare earth elements. Incomplete REE patterns were due to concentrations of some REE below the LOD. Rare earth element concentrations were normalized with respect to the Post Archean Average Shale (PAAS) standard (Taylor and McLennan, 1985).

4. Results

4.1. Petrographic description of diagenetic stages

The diagenetic sequence is given in figure 5 and the relative abundances of diagenetic features in the Middle and Late Jurassic limestones are listed in the Table 1.

4.1.1 Early diagenesis

As reported by Brigaud et al. (2009a), in Middle Jurassic limestones of the eastern Paris Basin, early cements represent less than 6% of the total cement volume, except below marine hardgrounds and exposure surfaces, where synsedimentary low magnesium calcite (LMC) cements (cal0) and formerly high magnesium calcite (HMC) cement locally fill a large fraction of the inter granular pore space. By rigidifying contacts between grains these synsedimentary cements prevented mechanical compaction, which may have resulted in porosity being preserved below these surfaces (Purser, 1980; Brigaud et al., 2010). In the Oxfordian limestones early cementation or dissolution is very rare.

Micritization and micritic early cements

These common synsedimentary phenomena appear as micritic biocorrosion fringes growing from the surface to the centre of grains (destructive micritization; Fig. 6a) or as a microbial crust between grains (constructive micritization) (Kobluk and Risk, 1977). Constructive micritization can lead to the cementation of the sediment by micritic bridges between grains. Under CL the micritic biocorrosions are usually slightly more luminescent than the unaffected parts of the grain.

Early inclusion-rich calcite cements

These cements are either isopachous fibrous cements (IFC) or inclusion-rich calcite syntaxial overgrowths around echinoderm debris. IFC are generally thin (< 100 µm), inclusion-rich, with cloudy (non-zoned) orange to dark brown luminescence (Fig. 6b). They mainly developed directly below bored surfaces in Middle and, to a lesser extent, Upper Jurassic limestones. Inclusion-rich syntaxial cements are synchronous with the IFC and exhibit the same petrographic characteristics (Fig. 6a).

Both syntaxial and isopachous inclusion-rich early calcite cements of the Middle Jurassic and Upper Jurassic limestones have been interpreted as recrystallized High Magnesium Calcite (HMC) cements which precipitated in oxygenated marine waters near the water/sediment interface, in the geochemical context of a calcite sea (Durlet, 1996; Vincent, 2001; Brigaud; 2009).

Early vadose cements

Meniscus and microstalactitic cements have been observed but are very scarce. They are either micritic, sparitic or constituted by micro-spar. Micritic meniscuses are mostly due (see above) to binding microbial activity (Beier, 1985; Calvet et al., 2003; Holail and Rashed, 1992; Webb et al., 1999) and so may form in both vadose and phreatic environments (Hillgärtner et al; 2001). In Late Jurassic limestones, meniscuses can be constituted by a mixing of micrite and microspar. In contrast sparitic and microsparitic meniscus cements have been observed in granular sediments below Middle and Upper Jurassic exposure surfaces (Fig. 6c). These cements are translucent and limpid in Plane Light (PL) and non-luminescent under CL. Other vadose cements such as pendant or microstalactitic cements have been documented by Purser (1989), Javaux (1992) and Brigaud et al. (2009a) in the Bathonian *Calcaires de Chaumont*. Scarce fibrous pendant cements also occur in the top of the *Pierre d'Euville Lérouville* and in the Oxfordian *Oolithe de Doulaincourt* (Fig. 6d).

Early inclusion-poor calcite cements (Cal0)

Just like inclusion-rich early calcite cements, inclusion-free early blocky calcite cements (Cal0) are scarcer in Upper Jurassic than in Middle Jurassic limestones. They form scalenohedral fringes, drusy spars and first bands of syntaxial cements. They are generally non-ferroan but early ferroan marine

cements have been described in the *Oolithe miliaire inférieure* (Brigaud et al., 2009a). Under CL, these cements are dull, dark or non-luminescent and occasionally display one or more thin yellow bands (Fig. 6e). In the Middle Jurassic, these cements mainly occur below major hardgrounds where they are crosscut by borings and sometimes associated with early dissolutions of calcite and aragonite bioclasts. Such hardgrounds have been interpreted as sequence boundaries which may record exposure events (Javaux, 1992; Durlet and Loreau, 1996; Brigaud et al., 2009b).

Aragonite-to-calcite neomorphism and aragonite dissolution

The internal structures of aragonitic organisms such as corals, gastropods or some bivalve shells are sometimes replaced by calcite. This neomorphic calcite consists in small non-ferroan and turbid anhedral spars (Fig. 6f), sometimes pleochroic, measuring less than 100 µm (average size about 20 µm). Under CL they are poorly luminescent (dark to brown) with an inconspicuous cloudy pattern. This neomorphic calcite differs from the zoned euhedral blocky calcite cements that usually precipitated in moulds due to (early) dissolutions of aragonite bioclasts (Fig. 6f).

4.1.2 Mesogenesis and telogenesis

Pyrite 1 (Py1)

Framboids and cubic crystals of pyrite (Py1) are relatively common, especially below and above drowning surfaces. Cross-cutting relationships show that these pyrite crystals precipitate after Cal0 in the Middle Jurassic limestones (Fig. 6b). This first generation of pyrite has not been observed in the Upper Jurassic limestones.

Mechanical compaction and fractures (F1)

Mechanical compaction is the spatial rearrangement and fracturing of grains affected by vertical loading during the first stages of burial. Evidence of mechanical compaction consists of fractured grains and spalled oolite. It is poorly developed where thick early cements rigidified the grain contacts. A first fracturing event (F1a) cuts across grains, matrix and early cements. Fracture widths never exceed 1 cm and their vertical extent is limited to less than 10 cm. Their orientations are random with a slight dominance of NE–SW directions (Fig. 9). They are filled by both Cal1 and/or Cal2 cements

(Fig. 6g). A second stage of fracturing (F1b) after the formation of microspar dykes has been observed mainly in the core of well A901. It consists in thin (< 300 µm wide) vertical and faintly sinuous veins.

Microspar-cemented fractures (Md)

Microspar-cemented fractures correspond to straight or slightly sinuous fissures. In outcrops they have a white 'milky' texture. They may be up to 5 cm wide and dykes are vertically continuous at the outcrop scale (several metres to several tens of metres). Fissures exhibit multiphase filling. The first phase of cementation corresponds to a non-ferroan and limpid equant calcite presenting a faint zoning and a dull orange luminescence under CL. The sizes of crystals ranges between 20 and 100 µm. Clasts of micritic matrix or isolated carbonate grains are often incorporated in this first cementation stage (Fig. 6h). The second cementation phase consists of non-ferroan microspar with dark laminations parallel to the fissure edges. The crystals are less than 10 µm in size. Matrix clasts are absent from this cement. In the Middle Jurassic limestones only two microspar-cemented fractures have been observed in the *Oolithe de Freville* in the Coussey quarry, oriented 40°N. In the Upper Jurassic limestones, they are present in several localities such as Sorcy, Void-Vacon, Maxey-sur-Vaise and Dugny-sur-Meuse (Fig. 1). They occur in mudstones of the *Calcaires coralliens de Sorcy*, *Calcaires coralliens d'Euville* and *Calcaires crayeux de Maxey* members (Fig. 4). In the Dugny-sur-Meuse quarry, moulds of corals are connected to microspar-cemented fractures and are filled by the same successions of cements (equant spar on the edges and microspar toward the centre). These fractures display a main direction of about 20°N (Fig. 9) except in the Dugny-sur-Meuse quarry where the main directions are 70°N and 14°N.

Calcite 1 (Cal1)

Cal1 consists of non-ferroan limpid crystals of LMC and displays a bright orange luminescence with faint concentric zoning (Fig. 6a, 6b, 7a, 7b). Cal1 constitutes the first blocky cement in intergranular and intragranular porosity and in some F1 fractures (Fig. 6g). This cement is posterior to the Py1 pyrites in the Middle Jurassic limestones (fig.6b). Crystals are large (up to 400 µm) and poor in small fluid inclusions. Contemporaneous syntaxial cements, with the same non-ferroan and luminescent bands, are usually thicker (up to 500 µm) (Fig. 6a).

Cal1 cements are only observed in Middle Jurassic limestones. Their relative ratio is variable depending on stratigraphic levels (0 to 95% of the porosity filling). In the northern quarry of Thin-le-Moutier in the vicinity of the Ardennes Massif, Cal1 cement constitutes more than 50% of the cementation (up to 95% in some samples). In 236 samples of Middle Jurassic cores from EST 433, EST 210 and HTM 102, this cement constitutes on average 35% of the total cement volume (Brigaud et al., 2009a).

Chemical compaction and stylolites 1 (Ccs1)

Chemical compaction is characterized by stratiform stylolites with vertical peaks and by microstylolites at the contact between allochems in non-early cemented grainstones. This first generation of stylolitization affects F1 and all the diagenetic phases up to the Cal2 calcite. Stylolites are present in all the Middle and Upper Jurassic limestones (cores EST 210, EST 204, EST 433 and A901), are well developed in mudstone facies and are widespread in the *Oolithe Miliaire* and *Calcaires de Dainville* member.

Dolomite 1 (Dol1)

The first generation of dolomite corresponds to 50–100 µm non-ferroan euhedral rhombs. These rhombs are more or less turbid depending on stratigraphic levels and usually contain small solid inclusions. Under CL, the complete dolomite crystal consists of two sub-zone growths: (1) a 10 µm orange luminescent euhedral core and (2) a relatively large (up to 200 µm) non-luminescent rim with a thin, bright red, external fringe (Fig. 7c). Rhombs presenting only the first dull orange luminescence sub-zone have been observed in the *Calcaires à polypiers supérieurs* of the Malancourt quarry and in *Oolithe miliaire* in the EST 210 core. Rhombs with only the second sub-zone are often observed, as in the *Calcaires de Chaumont* in EST 433 cores. Dol1 fills part of intergranular pore space and is concentrated with insoluble material in stylolites Ccs1 (Fig. 7d). Dol1 postdates Cal1 and predates Cal2 calcite.

Calcite 2 (Cal2)

Cal2 is limpid equant ferroan blocky calcite (Fig. 7e,g) and displays a dull brown luminescence (Fig. 6a,b and 7f,h) without any obvious zonation, except in local levels where a faint zoning can be

observed. Cal2 calcite has been observed in primary intergranular pores in grainstone facies (Fig. 6b and 7e,f,g) as well as in geodes (Fig. 6f) and in fissures F1 (Fig. 6g). Crystals are euhedral, limpid and up to 2 mm in size. In geodes Cal2 blocky calcite often shows a patchy flecked aspect. Cal2 is observed throughout the Middle Jurassic limestones, but in the Upper Jurassic it seems to be restricted to a few grainstone levels. Cal2 is affected by chemical compaction and is also present in relay zones of stylolites 1. The volume of Cal2 varies with the stratigraphic position. The percentage of Cal2 can reach 40% in the *Calcaires compacts de Neufchâteau* in the Bazoilles-sur-Meuse area (fracture cementation) and 60% in the *Oolithe de Jaumont* in the Jaumont area (intergranular cementation). In the Middle Jurassic cores EST 433, EST 210, A901 and HTM 102, this cement constitutes on average 35% of the total cement volume from 236 samples (Brigaud et al., 2009a). In the Upper Jurassic limestones, Cal2 occurrs essentially in the *Calcaires de Dainville* member where it never exceeds 20% of interganular cements and in the Upper Oxfordian *Oolithe de Saucourt inférieure* and *Oolithe de Saucourt supérieure* members where it may entirely fill the intergranular pore spaces (Fig. 7g).

Quartz 1 (Qz1)

Silicification is rare and has been observed in the Middle Jurassic *Calcaires à polypiers inférieurs* formation in the Malancourt quarry, in the carbonate layers of the *Marnes de Longwy* formation in core samples EST 210, and in the Dugny-sur-Meuse quarry in moulds of corals in the Upper Jurassic *Calcaires coralliens d'Euville* Member. It is also significantly present in the HTM 102 well, in the lower part of the carbonate-dominated *Foug* formation at the contact with the underlying Callovian–Oxfordian marly succession (Vincent, 2001). Silica occurs as euhedral quartz in geode infillings (Fig. 7i) or as chalcedony nodules replacing bivalve shells, sea-urchin spines or micritic matrix (Fig. 7j). In the Malancourt quarry euhedral quartz constitutes the last stage of geode cementation and clearly postdates Cal2 and neomorphic calcite but is prior to the second pyrite event and Cal3 cement. Quartz is crosscut by F3 fractures filled by Cal4 (Fig. 7j).

Fractures 2 (F2)

The second stage of fracturing (F2) corresponds to narrow (<15 µm wide), sinuous and vertical anastomosing fissures (Fig. 7h,k,l). These fractures are sometimes broad (about 2 cm wide) such as

in Upper Jurassic limestones where a main direction of about 20–40°N can be observed (Fig. 9). The vertical extent of the crack network can reach several metres. F2 fractures crosscut F1, Ccs1 Qz1, and Cal2, and they are filled by Cal3 (Fig. 7f,l,m). They are connected with intra-cortical spaces in some cracked oolites (Fig. 7k). Only desquamated parts of cortex display preferential stretching in a horizontal plane. Conversely, nuclei are generally stretched in a vertical plane. F2 fractures are only slightly impacted by or crosscut compaction stylolites (Fig. 7m)

Pyrite 2 (Py2)

The second episode of pyrite precipitation (Py2) consists of euhedral cubic crystals with a maximum size about 250 µm. It appears in primary intergranular pore spaces (Fig. 7h), in cracked oolites, in geodes, in moulds of corals, and on the edges of some F2 fractures. Crosscutting relationships show that Py2 precipitated after Cal2 but before Cal3 (Fig. 7h) in both Middle and Upper Jurassic limestones.

Calcite 3 (Cal3)

Cal3 blocky cements are non-ferroan (Fig. 7e) and display a bright orange luminescence with sector zoning under CL (Fig. 7f and 8a). The Cal3 calcite develops in continuity with Cal2 crystals or appears in the filling of F2 fractures. The crystals, which may reach 1 mm, are limpid and may contain one-phase liquid small fluid inclusions. Cal3 calcite fills the intergranular pore spaces, F2 fractures and some geodes. In the Middle Jurassic Cal3 cements fill intra-cortical spaces of cracked oolites connected with F2 (Fig. 7k). Cal3 entirely or partly fills the residual space between Cal2 crystals in the Middle Jurassic limestones. It accounts for between 0 and 15 % of the cementation in the Middle Jurassic and as much as 50% of the cementation volume in the Upper Jurassic (Fig. 8a). In the Middle Oxfordian geodes, Cal3 generally constitutes the first cementation event (Fig. 8a). Cal3 predates fluorite crystals and postdates euhedral Py2 pyrite crystals (Fig. 7h).

Fluorite 1 (Fl1)

CL observations display a blue luminescence. Fluorine may be anhedral when replacing calcite of echinoderms (*Oolithe de Doncourt*, A901 core), micritic matrix, allochems and all the previous cement stages Cal1, Cal2, Dol1 and Cal3 (Fig. 8b). In the *Calcaires crayeux de Gudmont* Member (Oxfordian),

fluorite occurs in sinuous veins and replaces micritic matrix, early cements and Cal3 cement. Evidence of replacement of these cement stages by fluorite was observed in the Malancourt quarry or in the EST 210 core. Fl1 is affected by compression stylolites (s2) (Fig. 8d). Replacement occurs on the edges of primary intergranular pores where early cements and grains may be affected (Fig. 8c). Fluorine is characterized by euhedral cubic crystals of up to 1.5 mm when precipitated in moulds of corals (*Oolithe de Jaumont* formation) (Fig. 8e) or in intergranular pores (*Calcaires à polypiers inférieurs* in Malancourt quarry, *Calcaires de Chaumont* in the EST 210 core). A transition from replacement fluorites on pore edges to euhedral crystals towards the centre of pores was often observed (Fig. 8c).

Fractures 3 (F3)

A final stage of fracturing is attested by straight and wide fractures. They may be as much as 4 cm wide and tens of metres in vertical extent. These fractures are rare and show a preferential direction of about 150°N in Middle Jurassic limestones and betwe en 120 and 140°N in Upper Jurassic limestones (Fig. 9). They crosscut stylolites 1 but are affected by stylolites 2. F3 fractures crosscut all the previous diagenetic features and are filled by Dol2 and Cal4 (Fig. 8c,f).

Stylolites 2 (s2)

Vertical stylolites with horizontal peaks affect all the previous diagenetic stages such as fluorite and F3 (Fig. 8d). Dark insoluble material is present in stylolites. The main orientation of stylolite peaks is between 130 and 180°N in Middle Jurassic limestones . The low number of measurements on oriented thin sections does not indicate any main direction for s2 in the Late Jurassic. The relative chronology between Cal3 and s2 has not been observed.

Dolomite 2 (Dol2)

Two distinct forms of Dol2 dolomite crystals can be found in the Middle and Upper Jurassic limestones. The first corresponds to a saddle ferroan dolomite occurring at the base of the Middle Jurassic series. Dol2 evolves at the top of the Middle Jurassic carbonate and in the Upper Jurassic carbonates into the second form which consists of a planar non-ferroan dolomite (Fig. 8j). The saddle dolomite crystals are non-luminescent under CL, and EDX analyses indicate a non-stoichiometric

dolomite (55.5 mol% CaCO3, 38 mol% MgCO3 and 6.5 mol% FeCaCO3). The second crystal form displays a bright red luminescence and can be observed as overgrowths of Dol1 (Fig. 8g) or alone in geodes, in intergranular pores or in F3 fractures (Fig. 8h,i,j). Dol2 is scarce in the Middle Jurassic, except in porous layers where it may make up 50% of the total cement volume. In the Oxfordian, Dol2 is often the only cement where Cal4 is dominant (Fig. 8i,j). The growth of Dol2 on the edges of F3 filled by Cal4 in fractures indicates that it predates Cal4 (Fig. 8h). Dol2 has also been observed in pressure solution and transfer zones of the second generation of stylolites (Fig. 8d).

Fluorite 2 (Fl2)

A second stage of fluorite precipitation consists of small euhedral fluorite crystals. They occur locally in F3 fractures crosscutting fluorite vugs or veins (Fig. 8c) and in relay zones of s2 stylolites (Fig. 8d). They have been observed mainly on fracture edges filled by the last generation of blocky calcite (Cal4). This distribution suggests that this second fluorite precipitation predates the last blocky calcites.

Calcite 4 (Cal4)

Non-ferroan Cal4 is the last generation of blocky calcite. It displays a dull brown luminescence with concentric zoning (Fig. 8h,i). Crystals are large (up to 3 mm), limpid and non-ferroan with scarce small solid inclusions. It post-dates Dol2 in interganular pores and in fractures. Cal4 also postdates fluorite in the *Calcaires à polypiers inférieurs* (Fig. 8e). It fills transfer zones of s2 (Fig. 8d) but F3 fractures filled by Cal4 can be affected by s2. This suggests that precipitation of Cal4 is at least in part coeval with compressive stylolitization. Cal3 and Cal4 constitute more than 90% or the entire cementation in coral moulds or intergranular pore spaces of the Middle Oxfordian limestones from the *Calcaires coralliens de Sorcy*, at the base, to the *Calcaires crayeux de Maxey* at the top (Fig. 8j). However, Cal4 is relatively scarce in Middle Jurassic limestones, where it constitutes less than 10% of the cementation volume and mainly develops in fractures F3, in the residual intergranular pores, and in moulds of corals.

4.2 Geochemical analysis

The Middle Oxfordian and Middle Jurassic limestones are vertically separated by the Callovian–Oxfordian clays and marls of the *Argiles de la Woëvre*, *Terrain à Chailles*, and *Marnes blanches des Eparges* Fm. (Fig. 4). On the Eastern margin of the Paris Basin the thickness of this interval varies between 220 m in the Verdun area to the north and about 100 m in the Neufchâteau area to the south (Carpentier et al., 2007). Considering a thermal gradient of 30 °C/km in the Paris Basin and a maximum burial temperature of 60 °C for the bottom of the Middle Jurassic (Blaise et al., this issue), the difference in temperature between Middle Jurassic and Oxfordian aquifers during burial was about 7 °C in the northern part of the basin. Using the oxygen isotope fractionation equation between inorganic calcite and H_2O determined by O'Neil et al. (1969), the $\delta^{18}O$ offset between Middle Jurassic and Oxfordian calcite cements precipitated from the same parent fluid at a maximum temperature of 60 °C and with a range of 7 °C could reach 1.2‰. Al so, due to the uplift of the northern part of the basin during Cretaceous times (Guillocheau et al., 2000), greater burial temperatures may be considered in the southern part of the study area (Neufchâteau) for a given stratigraphic interval. Despite these differences, the integration of published data with the results obtained in this study allows us to propose a coherent scheme merging the various blocky calcite cements identified in both the Middle Jurassic and Oxfordian limestones. Geochemical data are listed in supplementary material Appendix A, including the sample name, location, cement type, and the $\delta^{18}O$ and $\delta^{13}C$ values.

Md - Measured $\delta^{18}O$ values on Md range from –7.2‰ to –6.2‰ with a mean value of –6.7‰, and $\delta^{13}C$ values range from 0.9 to 1.8‰ with a mean value of +1.3‰ (Fig. 10a).

Cal1 – Cal1 was observed and analysed only in Middle Jurassic limestones. This calcite displays low $\delta^{18}O$ values ranging from –6.0 to –3.5‰ with a mean value of –5.0‰ (Fig. 10a). The range of $\delta^{13}C$ values on Cal1 fluctuates from +1.6 to +2.5‰ with a mean value of +2.2‰. REE analyses of Cal1 are not conclusive since REE concentrations are below detection limits.

Dol1 - Dol1 ranges between –4.0 and –2.0‰ for $\delta^{18}O$ and between +2.5 and +3.0‰ for $\delta^{13}C$. Dol1 dolomite is slightly depleted in LREE with no apparent Ce anomaly (Fig. 11). Dol1 dolomite has higher Sr and lower Mn and Fe contents than Cal2 and Cal3 (Fig. 11). The Mg/Ca ratio ranges between 0.44 and 0.48.

Cal2 - Oxygen isotope values on Cal2 range from –8.0 to –6.7‰ with a mean value of –7.3‰, and $\delta^{13}C$ values are from +0.2 to +2.8‰ with a mean value of +1.3‰ (Fig. 10a). Cal2 cements display flat or slightly Light Rare-Earth Element (LREE)-depleted patterns at 0.1 times the PAAS (Fig. 11). Some profiles show a Gd crested 'chevron' pattern (*sensu* Azmy et al., 2011). Calcite is Fe enriched (2300 to 4250 ppm) and rather depleted in Mn and Sr (<350 and 400 ppm respectively). Mg contents range between 1100 and 2540 ppm.

Cal3 - Measured $\delta^{18}O$ values on Cal3 range from –8.7‰ to –7.7‰ with a mean value of –8.0‰. $\delta^{13}C$ values on Cal3 range from +0.7 to +3.4‰ with a mean value of +1.9‰. REE patterns of Cal3 are often incomplete (Fig. 11). Despite this limitation, two typical REE patterns are evidenced. The first corresponds to a flat, shale-like or slightly LREE-enriched pattern. ΣREE and Fe contents (<800 ppm) are lower than for Cal2. Mg values range from 740 to 1500 ppm. Mn and Sr contents never exceed 260 and 140 ppm respectively. The second trend displays depletion in LREE with a negative Ce anomaly. Compared with Cal3 calcite which presents a flat REE pattern, the LREE-depleted calcite is Mg- and Mn-enriched. Fe and Sr contents are in the same range of values as in Cal3 with a flat REE pattern.

Fl1 is characterized by a gradual enrichment from LREE to HREE with a Ce negative anomaly (Fig. 11). Mg and Sr values can vary over eight to ten orders of magnitude, respectively. Mg is positively correlated to Sr. Fe contents range over about 850 ppm.

Dol2 cements display a flat LREE to MREE distribution with a slight depletion in HREE. However, an apparent negative Ce anomaly is observed (Fig. 11). ΣREE content is higher than in Cal3 and Cal4. Mn and Fe content is low, while Sr is higher than for Cal2 and Cal3. The Mg/Ca ratio is between 0.42 and 0.48.

Cal4 - Measured $\delta^{18}O$ values on Cal4 range from –11.8‰ to –8.0‰ with a mean value of –8.9‰. $\delta^{13}C$ values range from +0.9 to +3.1‰ with a mean value of +2.2‰. The range of $\delta^{18}O$ values of Cal4 in Middle Jurassic limestones (-9.2‰) is, however, larger than the range of Oxfordian limestones values

(-8.5‰; Table 2). In the Middle Jurassic Cal4 calcite shows high ΣREE contents. The complete profiles are slightly depleted in LREE with systematic apparent negative Ce anomaly (Fig. 11a). In the Late Jurassic Cal4 displays an LREE-depleted pattern with a gradual increase in MREE and HREE content (Fig. 11b). Their Fe content is lower than Cal2 cements. Mg content is highly variable and fluctuates over three orders of magnitude. The Mn content is very low while Sr content can exceed 1300 ppm. However, Sr is depleted in Cal4 crystals characterized by the lower ΣREE content.

5. Discussion

5.1 Timing of fracturing

Despite a slight NE–SW dominance, no clear preferential orientation is observed for F1 fractures. From this observation, we infer that fracturing was not generated under a single, dominant tectonic regime with a constant stress field. Fractures observed in the Middle Jurassic predate Cal1 calcite and stratiform stylolites 1. These features indicate that F1 formed before the maximum burial of the basin in the Late Cretaceous (Guillocheau et al., 2000). On the one hand, the limited vertical extent of these fractures (less than 10 cm) suggests that they may be linked to mechanical compaction during the first stages of burial. On the other hand, very early fractures that affected early cemented Lower Bajocian limestones located near synsedimentary extensional faults have been documented in the south-eastern part of the Paris Basin (Durlet et al., 1997). Such a tectonic origin for some F1 fractures is not attested here where synsedimentary faults are not documented in the vicinity of sampled drill cores or quarries.

Microspar-cemented fractures (Md) usually correspond to the first generation of fractures in both Middle Jurassic and Oxfordian limestones. The alternating pattern of microsparitic and sparitic cements underlined by micritic laminations and the occurrence of intraclasts and carbonate grains trapped in the first stages of calcite spars indicates successive phases of fracture opening in poorly indurated sediment. All these features are similar to those described by André et al. (2004) in sedimentary dykes of the eastern Paris Basin. General orientations measured in this work and their local changes in the Dugny-sur-Meuse area are consistent with directions reported in André et al. (2004) (Fig. 9). $\delta^{18}O$ and $\delta^{13}C$ values measured on microspar-cemented fractures are also similar to

those obtained by those authors (Fig. 10b). The early origin of these dykes in the paragenesis of both Middle Jurassic and Oxfordian limestones is consistent with a late Jurassic age (late Oxfordian to Kimmeridgian) proposed by André et al. (2004).

The rather low number of direction measurements on F2 fractures in Middle Jurassic limestones that are filled only by Cal3 cements precludes any discussion of a preferential orientation of fractures. However, since only desquamated parts of cortex display preferential stretching in a horizontal plane and nuclei are generally stretched in a vertical plane, cracked oolites do not seem to be linked to mechanical compaction but rather to the propagation of vertical fractures in weak zones of oolite cortex. This suggests that F2 fractures in Middle Jurassic limestones were generated by a dominant horizontal strain. The compressive Pyrenean phase that started during the Late Cretaceous and continued until the Oligocene in the Paris Basin (André et al., 2010) may be responsible for F2 fracturing.

In the Oxfordian limestones, F2 fractures display a preferential orientation between 20 and 40°N. The Oligocene extension is recorded in the eastern Paris Basin by several graben such as the Gondrecourt and the Joinville grabens. In addition, several studies showed that Pyrenean stress-fields are recorded in the Anglo-Parisian Basin (André et al; 2010; Lacombe and Obert, 2000; Mortimore and Pomerol, 1997). 20 and 40°N directions are consistent with both compressive Pyrenean and extensional Oligocene directions. However, there is no evidence for favouring one or other tectonic event.

Wide F3 fractures with a large vertical extend are filled by the second generation of dolomite (Dol2) and Cal4 cements. However, Dol2 is not systematically encountered. In Middle Jurassic limestones F3 fractures correspond to the telogenetic F2 fractures described by Brigaud et al. (2009a). F3 fractures display preferential orientations of respectively 140°N and 150°N, typical of Alpine compression strains in the Paris Basin (André et al., 2010). F3 fractures are affected by horizontal stylolitic peaks or are associated with them, suggesting that these fractures formed during Oligocene times and continued to form during the Miocene when Alpine strains predominated.

5.2 Blocky calcite cements in Middle Jurassic and Oxfordian limestones: towards a common paragenetic scheme

The spatiotemporal distribution of early cements (Cal0 and IFC) was controlled by numerous factors such as sediment texture, sequence stratigraphy and depositional environments. These cements represent only between 0 and 20% of the total poronecrosis, except below marine hardgrounds and exposure surfaces where they are more abundant. Although their occurrence may have partly inhibited compaction during burial (Heydari, 2003), initially porous granular sediments are currently sealed due to intensive cementation by blocky calcites. As a consequence the discussion will focus on the timing and the origin of mesogenetic and telogenetic blocky cements which are responsible for the major volume of porosity loss in Jurassic limestones of the eastern Paris Basin.

5.2.a Meteoric vs marine fluids

The Jurassic was a period of calcite seas (Sandberg, 1983) so that after the death of organisms aragonite was unstable in sea water (Palmer et al., 1988). Dissolution or transformation affects aragonite when sea water is slightly or greatly undersaturated with respect to aragonite. Consequently mouldic dissolution of aragonite and aragonite-to-calcite neomorphism probably started during early diagenesis in oxidizing environments as suggested by the non-ferroan composition and the lack of luminescence of the core of neomorphic calcite. Neomorphism of aragonite to calcite from marine or meteoric waters is also efficient during the initial stages of burial in a closed system (marine-burial environment of Melim et al., 2002). The final stages of aragonite-to-calcite neomorphism are characterized by a bright yellow luminescence, suggesting that neomorphism continued in a slightly reducing environment during early burial that allowed scavenging of Mn^{2+} in the calcite lattice. Negatively shifted $\delta^{18}O$ values of neomorphic calcites measured by Vincent et al. (2007) compared with bivalve shells are consistent with a transformation during shallow burial or in a shallow meteoric aquifer (Fig. 10b). However, during shallow burial a greater renewal of marine or meteoric waters in an open system would cause mainly dissolution of aragonite (Melim et al., 2002). As a consequence, depending on the rate of water renewal during shallow burial, aragonite neomorphism was accompanied by a more or less extensive formation of moldic porosity in corals. The infill of some

Bajocian and Bathonian geodes by Cal1 and Cal2 calcites also argues for the appearance of geodes during the initial stages of burial, or even earlier when inclusion-rich (HMC) and inclusion-free early calcite cements (Cal0) filled dissolved aragonitic bioclasts. Either marine waters or meteoric waters could have generated these early dissolutions of biogenic aragonite.

$\delta^{13}C$ values of blocky calcite cements are usually higher in Oxfordian limestones than in Middle Jurassic limestones (Fig. 10a). In buried limestones, the carbon isotope composition of pore fluids is usually buffered by the surrounding carbonates (see, for example, Anderson and Arthur, 1983; Moore, 2001). As a consequence, the $\delta^{13}C$ values of blocky calcite cements described here are not used for interpreting the fluid sources.

As explained by André et al. (2004), microspar dykes formed early, between the Middle Oxfordian and the Late Tithonian. Such timing is in agreement with our observations. Considering low temperatures of precipitation between 25 and 35 °C at the end of the Late Jurassic (Fig. 12) and with a $\delta^{18}O$ of Md calcites between -6 and -7‰, the parent fluid composition ranges between –2‰ to –6‰ (SMOW) (Fig. 13). Such a parent fluid composition is characteristic of nearly pure freshwater. André et al. (2004) interpreted the $\delta^{18}O$ values as early inputs of freshwater during Oxfordian subaerial exposure or later during the LCU. The more meteoric signature of Md calcites compared with subsequent burial cements (see below) suggests that synsedimentary surfaces of subaerial exposure were probably responsible for infiltration of the parent fluids.

Recent U/Pb dating of blocky calcite in Middle Jurassic geodes by Pisapia et al. (2011) indicates an age of 149.2 ± 5.8 Ma. This age can be attributed to Cal1, Cal2 or to a mix of both calcites. Since Cal1 and Cal2 generally occur together in Middle Jurassic geodes, the U/Pb dating is most probably an average value between the two blocky calcite zones. In this case, Cal1 may be older and Cal2 younger than the age range suggested.

Cal1 formed prior to pressure solution and precipitated during early burial. Assuming a maximum burial temperature of about 60 °C at the base of Middle Jurassic limestones during the Late Cretaceous and a Late Jurassic–Early Cretaceous age (before the maximum burial and the maximum

of chemical compaction) for Cal1, a temperature range between 30 °C and 40 °C for the precipitation is realistic (Fig. 12). For lower $\delta^{18}O$ V-PDB values of Middle Jurassic Cal1 cements (–6‰), with a temperature range of 30–40 °C, the parent fluid com position ranges from –1‰ to –3‰ (SMOW). $\delta^{18}O$ of the parent fluid is slightly depleted compared with sea water (0‰ SMOW for sea water according to Lécuyer et al., 2003), (Fig. 13). The U/Pb datings imply that inputs of freshwater occurred during early burial between the Late Jurassic and the Early Cretaceous. In this case Cal1 can be correlated with the entrance of freshwater into the system during the LCU as stated by Brigaud et al. (2009a). The parent fluid composition consisted in (1) a mixing between trapped Middle Jurassic marine waters and subsequently-introduced, isotopically-depleted meteoric water, or (2) in meteoric water buffered during circulation in Jurassic carbonate, as suggested by Brigaud et al. (2009a).

Cal2 is affected by pressure solution and appears in relay zones of stylolites. These features indicate that Cal2 is coeval with burial stylolites. With the dating proposed by Pisapia (2011), a temperature range during the Early Cretaceous slightly higher than for Cal1 can be envisioned with a range between 30 and 50 °C (Fig. 12). The average $\delta^{18}O$ values for Cal2 in Middle Jurassic and Upper Jurassic limestones is respectively of –7.3‰ and –7.2‰. With this temperature range and Cal2 $\delta^{18}O$ values, the isotopic signature of the parent fluid ranges from –4‰ to 0‰ (SMOW). For lower $\delta^{18}O$ V-PDB values of Middle Jurassic Cal2 cements (-8‰) (Fig. 10), with a temperature range of 35–50 °C in the Middle Jurassic limestones (Fig. 12), the parent fluid composition ranges from –1‰ to –3‰ (SMOW) and implies a contribution of meteoric fluids (Fig. 13). For $\delta^{18}O$ V-PDB values of Upper Jurassic Cal2 cements (–7.3‰) (Fig. 10), with a temperature range of 30–40 °C in the Upper Jurassic limestones (Fig. 12), the parent fluid composition ranges from –2‰ to –4‰ SMOW (Fig. 13). This suggests inputs of freshwater into deep aquifers before the maximum burial of the basin. Since no intensive vertical fracturing event occurred before the Pyrenean compressive phase, inputs most probably occurred by lateral recharge. Such a fluid pathway implies the aquifer cropped out on the basin edges. This configuration prevailed during the LCU and LAU.

Cal3 probably precipitated during the Pyrenean compressive event and/or during the Oligocene extension. The Pyrenean phase began during the Late Cretaceous and continued until the Eocene during the exhumation of the basin. As a consequence, the age of Cal3 is not well constrained. The

Late Cretaceous corresponds to the maximum burial of the basin. Due to the age uncertainty, a large range of temperatures between 60 °C and 30 °C durin g late burial and subsequent exhumation can be considered (Fig. 12). At these temperatures, the composition of the parent fluid ranges from 0 to –5‰ (SMOW). Thus the $\delta^{18}O$ values of Cal3 are not in agreement with low-temperature precipitation from pure sea water (Fig. 13). A contribution of meteoric fluids must be contemplated. Such inputs were certainly favoured by the vertical fracturing (F2 fractures) and inputs from deep aquifers or from the surface.

Based on fluid inclusions analysed by Buschaert et al. (2004), the temperature of precipitation of Cal 4 in Oxfordian limestones was between 32 and 42 °C. T he $\delta^{18}O$ of Cal4 is similar to that of calcite filling Oligocene faults of the Gondrecourt graben (Buschaert et al., 2004). Values are also similar to Alpine tension gashes measured by André et al. (2010) in the eastern Paris Basin. This is consistent with observations of Cal4 in the youngest fractures with orientations compatible with the Alpine main strain. Cal4 calcite filling vugs in the Oxfordian limestones were dated by the U/Pb method at 33.2 ± 5.5 Ma, corresponding to the Late Eocene / Oligocene period (Pisapia et al., 2011). Considering a telogenetic origin during the Alpine phase and a range of temperatures between 30 and 45 °C (Fig. 12), $\delta^{18}O$ values of Cal4 indicate that it precipitated from meteoric fluids (–4 ‰ SMOW). The results of the present study show that, for the Middle Jurassic, most depleted $\delta^{18}O$ values for Cal4 around –10‰ correspond to samples from Bazoilles-sur-Meuse (Fig. 1) located in the southernmost part of the study area (Fig. 1). This trend is absent from the Oxfordian because the sampling zones are located north of the Middle Bajocian ones. The results of André (2003) on Tertiary tension gashes show the same trend with the lowest $\delta^{18}O$ values in samples from south of the Marne Valley (Fig. 10c). It is noteworthy that Vincent et al. (2007) report some low $\delta^{18}O$ (below -10‰; Fig. 10b) for late burial assimilated to Cal4. Values obtained by Brigaud et al. (2009a) show an overall negative shift in Middle Jurassic $\delta^{18}O$ values (main value about –9.9‰) compared with the present study (main value about –9.2‰) (Fig. 10). Most of these samples were collected in the area of Chaumont and Neufchâteau located south of the study are or in its southern part (Fig. 1). Despite lower values corresponding to samples of the EST 210 drill core, this southern origin of samples is in agreement with a southward decline in the $\delta^{18}O$ signal. About 50 km south of the study area, a more depleted $\delta^{18}O$ value (-13.6‰ PDB) is also reported by Durlet (1996) in the latest blocky calcite zone (probably equivalent to Cal4) in the

Calcaires à polypiers inférieurs of the Pouillenay quarry. This regional trend may be due to an increase in temperature towards the south during precipitation of Cal4 or to inputs of meteoric waters from the southern part of the basin. These hypotheses are discussed below.

5.2.b Water/rock ratio and redox conditions

The Ce-Anomaly

First of all, the existence of a Ce anomaly on REE patterns must be evaluated since Bau and Dulski (1996) consider that apparent negative Ce anomalies on REE spectrums may reflect positive La anomalies. According to those authors, by comparing Ce anomalies (Ce/Ce*) with the Pr/Pr* ratio it is possible to differentiate between real Ce anomalies and La anomalies (Fig. 14a). There is no Ce anomaly for mesogenetic calcite represented by the blocky calcite Cal2 and the dolomite Dol1. A negative Ce anomaly appears for telogenetic calcite Cal3, calcite Cal4, dolomite Dol2 and fluorite Fl1. It should be underlined that no REE pattern shows a positive Ce anomaly, meaning that there was no deposition of REE in oxidizing conditions in which Ce^{3+} could be oxidized to Ce^{4+} as shown by Braun et al. (1990) in laterites.

REE behaviour during the mesogenetic stage

Since no fractionation of REE occurs during calcite precipitation (Nothdurft et al., 2004; Webb et al., 2009; Wyndham et al., 2004), the REE pattern of calcite directly reflects the composition of the parent fluid. REE patterns of Cal2 are enriched in LREE, MREE and global ΣREE compared with the REE profile of Oxfordian bottom sea waters determined by Olivier and Boyer (2006; Fig. 11). Cal2 calcite displays very low or no negative Ce anomalies and a slight La positive anomaly in some samples (Fig. 14a). The Ce content in sea water is controlled by the redox potential (Ballanca et al., 1997; Banner et al., 1988; Bau and Dulski, 1996; Denniston et al., 1997; Elderfield, 1988; Palmer, 1985; Shields and Stille, 2001). Ce is oxidized as Ce^{4+} in shallow sea water. Ce^{4+} is scavenged by Fe and Mn oxi-hydroxides and consequently is depleted in sea water. Haley et al. (2004) proposed that in reducing environments, interstitial waters are strongly enriched in MREE by the release of REE during the reduction of Fe-oxides. Reducing conditions certainly favoured the release of Ce during precipitation of Py1 (Haley et al., 2004) and the enrichment of Ce in the parent fluid of Cal2. The similar Sr content

between micritic ooids, peloids or matrix and Cal2 calcite suggests a low fluid/rock ratio (Brand and Veizer, 1980; Webb et al., 2009). The fluids that entered the aquifers on the southern margin of the Ardennes Massif during the LAU gradually became oversaturated with respect to calcite by dissolution of host carbonates as they percolated through the vadose zone. Oversaturation allowed calcite precipitation in the aquifer in the vicinity of the reload zone. Conversely, in the deep aquifer, chemical compaction was certainly an efficient additional mechanism that permitted oversaturation of pore fluids.

Furthermore, interactions with siliciclastic material (Allwood et al., 2010; Leybourne et al., 2000; Murray et al., 1990; Nothdurft et al., 2004; Pattan et al., 2005; Scherer and Seitz, 1980; Schieber, 1988; Webb and Kamber, 2000) can also erase the negative Ce anomaly hosted in the marine carbonate phase (Banner et al., 1988; Murray et al., 1990). Brigaud et al. (2009a) envisioned a reload of deep Middle Jurassic aquifers with meteoric waters from the subaerial exposures of the northern margin of the basin during the LCU and LAU. The weathering of plutonic, volcanic and metamorphic rocks, as well as the erosion of significant thicknesses of clay-rich formations on the Ardennes Massif may have generated REE enrichment of meteoric fluids (Leybourne et al., 2000). However, the Ardennes Massif was located more than 100 km north of the studied area and the reduced mobility of REE at low temperature is in disagreement with the hypothesis of REE enrichment of fluids of the deep aquifer by weathering of the basement. Conversely, the REE content of host micrites of carbonate grains, where Cal2 precipitated, displays a flat or slightly MREE-enriched pattern with a high ΣREE content. The host rocks exhibit no negative Ce anomaly (Fig. 14b) and are rich in Mg (Fig. 11c). The high Al and Fe contents suggest that terrigenous minerals are actually responsible for LREE and ΣREE enrichment and the lack of Ce negative anomaly compared with sea water. As a consequence the REE composition of Cal2 appears to be closely controlled by the host rock. Such a connection is consistent with an intensive contribution of pressure solution during the Cal2 precipitation since a siliciclastic content of just 1% is able to perturb the original REE pattern of sea water (Olivier and Boyet, 2006). In contrast, host rocks devoid of Cal2 calcite show a sea water-like pattern with slight ΣREE enrichment and a negative Ce anomaly (Fig. 14b). Their Al and Fe contents are low. This argues for a smaller siliciclastic input and lower clay content than in carbonates where

Cal2 precipitated. Consequently, the main source of REE in Cal2 is the clay content diluted in host carbonate which provided REE locally in fluids during pressure solution.

Pre-existing anisotropies can promote the appearance of stylolites (Bathurst, 1987). Clay minerals in limestones act as a catalyst for chemical compaction (Aharonov and Katsman, 2009). Systematic calcimetric measurements performed every two metres during the drilling of the EST 204 and EST 205 boreholes showed that the facies affected by chemical compaction present lower carbonate contents than the less compacted levels. This is particularly obvious in the non-porous and compacted *Calcaires de Dainville* member (Fig. 4) where clay interbeds are common at the top of metric parasequences (Carpentier et al., 2010). In addition Cal2 cements in intergranular macroporosity are correlated with the intensity of chemical compaction in the Oxfordian of the EST 204 and EST 205 boreholes (Fig. 15). Cal2 precipitated in intergranular porosity in sediments with a packstone/grainstone to grainstone texture. Some strongly stylolitized intervals do not display Cal2 because of their matrix-supported textures (mudstone to packstone) and the absence of initial macroporosity. Also, grainstone intervals devoid of chemical compaction-related features are also devoid of Cal2 calcite. Brigaud et al. (2009a) envisioned a possible high rock–water interaction influence for the parent fluid of Cal2 on the basis of Sr isotopes. This is consistent with the REE results. In addition, the high Mg content of Cal2 is compatible with a release from Mg-enriched host rocks during pressure solution. In summary, Cal2 precipitated during burial from mixed marine-meteoric parent water enriched in REE in a reducing environment and with a low fluid/rock ratio. The REE enrichment is linked to the ejection from clay material diluted in host rock pressure solution.

<u>REE behaviour during the telogenetic stage</u>

Cal3 cements are characterized by two types of REE patterns corresponding to (1) flat or LREE-enriched patterns and (2) LREE-depleted patterns with a negative Ce anomaly. The alternation of the two types of REE profiles is correlated with the zoning observed under CL. Depletion in LREE and negative Ce anomalies in some growth stages of Cal3 suggest a rather high water/rock ratio and the dissolution of carbonate minerals with a negative Ce anomaly which have precipitated from sea water. According to the data obtained about the mesogenetic calcite, the dissolution of calcite in grainstones

could explain the REE pattern; the lower ΣREE content suggests a decrease in the contribution by siliciclastic sources compared with Cal2 calcite. During this Cal3 stage there was alternation of fluid flows with different water/rock ratios and equilibration with different host rocks.

Cal3 calcite is linked to Pyrenean or Oligocene fractures. In the Paris Basin, the first record of the Pyrenean tectonic deformation lasted from the Late Cretaceous to the Eocene period (André et al., 2010; Vandycke, 2002). Cal3 cements are Fe-depleted compared with Cal2. On the question of Cal3 calcite exhibiting flatter REE patterns, low Fe content may be related to the prior precipitation of pyrite and release of Ce. In addition, the decrease in chemical compaction during telogenesis and the input of freshwater via fractures explain the diminution of ΣREE content in Cal3 compared with Cal2.

In the Oxfordian, Cal4 is characterized by a sea water-like REE pattern (Fig. 11b) with a negative Ce anomaly (Fig. 14a). These profiles are similar to those obtained by André (2003) for Pyrenean and Alpine tension gashes. Cal4 calcites are ΣREE-enriched in the Middle Jurassic compared with the Oxfordian. This is linked to the local control by host rocks since Middle Jurassic matrix and grains are richer in terrigenous minerals. Such enrichment argues for a dissolution phase of the host rock during Cal4 cementation. This dissolution phase may have enhanced geode porosity in Oxfordian limestones. Meteoric waters are generally under-saturated with respect to Low Magnesian Calcite (LMC) and generally CO_2-enriched due to soil weathering, these waters then being able to dissolve calcite (Sterpenich et al., 2009). Other dissolution mechanisms are pressure solution by Alpine stylolites. Nevertheless, in the Middle Jurassic Cal4 calcite exhibits a slight negative Ce anomaly (Fig. 14a) which is absent from host rocks. However, it is necessary to dissolve only the calcite grains or matrix to obtain a sea water-like REE pattern. This anomaly is not visible in the host rocks because it is masked by REE from detrital material. This is consistent with $^{87}Sr/^{86}Sr$ values being higher than those of bulk host limestones (Blaise, 2012) which also suggests rather high fluid/rock ratios and an intensive renewal of fluids. Such conditions are in agreement with infiltration of meteoric fluids from the surface along Oligocene and Alpine fractures as proposed by Buschaert et al. (2004) and André et al. (2010).

5.2.c Origin of dolomites

Dol1 dolomites were observed in the vicinity of stylolites or within them. A genetic connection between pressure solution and the first dolomite was proposed by Vincent et al. (2007). Brigaud et al. (2009a) also envisioned precipitation directly linked to chemical compaction and release of Mg from smectite on the basis of $^{87}Sr/^{86}Sr$ values. As for Cal2, flat REE patterns without a Ce anomaly suggest that REEs were released from adjacent host rocks and incorporated in the dolomite crystal lattice without any fractionation. The higher Sr content than in Cal2 also suggests that this element was transferred from host rocks to authigenic dolomite during the pressure solution process. This genetic connection between pressure solution and Dol1 explains the low Mg content of Cal2 compared with the host rocks, since this element was scavenged during the crystallization of dolomite.

The second generation of dolomite displays a flat REE pattern (Fig. 11) with a negative Ce anomaly (Fig. 14a). As with Dol1, the LREE and ΣREE enrichment of Dol2 is probably due to water/rock interactions with detrital minerals and marine calcite. Brigaud et al. (2009a) proposed that saddle Dol2 crystals in Bajocian limestones may form from upward hydrothermal flow at temperatures higher than 50 °C. If this is true, the lack of a positive Eu anomaly indicates temperatures lower than 100 °C and/or oxidizing conditions (Uysal et al., 2007). Upward flows of Triassic saline waters towards the Middle Jurassic aquifer during the Cenozoic period have been documented in the centre of the Paris Basin on the basis of Sr isotopes and the occurrence of saline fluid inclusions in the Middle Jurassic blocky cements (Demars and Pagel, 1994; Worden and Matray, 1995). However, the enrichment in ^{87}Sr may also originate from surface or sub-surface interactions with siliciclastic minerals in rocks or in soils. In addition, in the eastern Paris Basin, fluid inclusions in Cal4 calcite which postdates Dol2 display negligible chlorine content, showing that waters have not interacted with the Upper Triassic halite layers (Blaise, 2012). This discrepancy between the centre and the eastern margin of the basin suggests that the less-buried eastern margin was more influenced by meteoric water flows than the centre of the basin.

In addition, Dol2 is associated with horizontal stylolitic peaks affecting fluorite. Dol2 is also present in Alpine tension gashes. As with Dol1, pressure solution may be the source of Mg released in interstitial

waters. Pressure solution concentrated insoluble clay minerals in stylolites that released REEs which were subsequently incorporated in the adjacent newly-formed dolomite.

5.2.d Origin of pyrites

While the precipitation of Py1 can be easily attributed to the degradation of organic matter during the first stages of burial, several hypotheses can be proposed for the precipitation of pyrite between Cal2 and Cal3. On the one hand, the activity of sulphate-reducing bacteria can lead to the formation of pyrite, this process being known as BSR (bacterial sulphate reduction). This implies that sulphur was already present in the environment. However, no sulphur or sulphide mineral precipitation earlier than Cal3 has been observed despite the reducing conditions during burial favourable for sulphide precipitation. On the other hand, sulphur inputs may be envisioned for the Fe-sulphide formation coeval or prior to Cal3 calcite while they did not form during Cal2 precipitation despite the high Fe^{2+} content of pore waters. Such inputs may originate from the advent of sulphate-rich waters after the dissolution of Purbeckian evaporites. Another source of sulphur could be the migration of H_2S. If diluted in water such arrival implies an acidification of waters but the lack of dissolution coeval or prior to pyritization suggests that if such a migration occurred H_2S was in a gaseous state. In the Paris Basin the source rocks reached the oil window during the early Cenozoic, and a Paleocene to Oligocene age of migration is generally accepted (Espitalié et al., 1987; Pinti and Marty, 1995). This period corresponds to the defined potential window of precipitation of Cal3. However, until now, no H_2S migration has been documented in the Paris Basin. Analyses of sulphur stable isotopes in pyrite may be useful to determine their origin. In any case, such sulphur arrival may be linked to the appearance of new preferential fluid pathways. The occurrence of Py2 on the edges of Pyrenean or Oligocene tension gashes suggests that this network of fractures under compressive or extensional strains potentially created such pathways. The fact that Cal3 constitutes the first blocky cement in many Oxfordian limestones (geodes mainly) which were previously disconnected from fluid flows by surrounding micritic limestones is also in agreement with the appearance of new fluid pathways .

5.2.e Focus on the fluorite stage

In the Oxfordian limestones, the parent fluid of fluorite was undersaturated with respect to fluorite since in it first growth stage fluorite did not precipitate directly in pores but by replacement of host carbonates. Ca^{2+} was directly provided by the replaced limestones without release in the pore waters. Fluorite exhibits a sea water-like REE pattern. Since no fractionating of REE occurs during fluorite crystallization (Webb et al., 2009), the REE patterns of fluorite are directly the signature of host marine carbonates. These features argue for an opening of the system and inputs of new fluids undersaturated with respect to calcite. After growth by replacement, fluorite also precipitated directly as euhedral crystals in the pore space. This implies that Ca^{2+} was abundant enough in solution to permit euhedral fluorite precipitation.

The origin of the fluorite is still unknown. Brigaud et al. (2009a) proposed vertical fluid flows that weathered basement rocks and Lower Jurassic and Triassic marls. Those authors proposed that Oligocene extension was the most favourable geodynamical context for promoting such upward fluid flows. This model is consistent with our observations showing that fluorite postdates burial Cal2 cements and is crosscut by Alpine tension gashes. Such hydrothermal circulations generating saddle dolomite and fluorite precipitation have been described for several basins (Machel, 1999; Nesbitt and Muehlenbachs, 1997). However, LREE enrichment is thought to occur in fluids that weathered crystalline basement rocks (Leybourne et al., 2000). Conversely, euhedral Oxfordian fluorites show a sea water like REE pattern depleted in LREE. Consequently, a downward flow of meteoric fluids from the surface may have mobilized fluorite from overlying deposits and the origin of fluorite may also be sought in Purbeckian fluorites or Kimmeridgian clays. To the northeast, present-day water in the Oxfordian aquifer is enriched in sulphates due to the erosion/remobilization of Purbeckian evaporites during the retreat of the cuesta relief (Lindar et al., 2011). Fluorides are also present as leachable anions in Callovian–Oxfordian clays between both aquifers (Gaucher *et al.*, 2004). As a consequence, other sources of fluorine could be clay formations intercalated with or overlying Middle and Upper Jurassic aquifers (e.g. Kimmeridgian marls, Bajocian ‘Marnes à Ostrea acuminata’).

Finally, it should also be noted that fluorine may originate from the dissolution of fluorapatite. This mineral crystallizes during early diagenesis of marine carbonates (Rude and Aller, 1991) but is dissolved by low-temperature meteoric waters (Tribble et al., 1995; Chaïrat et al., 2007; Bengtsson et

al., 2007; Zhu et al., 2009). In this study, fluorapatite may have been dissolved since the meteoric water recharge during the Cretaceous. Fluorine releases from the dissolution of fluorapatite may have subsequently crystallized in fluorite thanks to the local uptake of Ca in host limestones.

5.3 Synthesis

The comparison of diagenesis in both Middle Jurassic and Oxfordian limestones of the eastern Paris Basin suggests the following overall scheme. Aragonite stabilization in LMC, accompanied by the appearance of geode porosity, occurred during early diagenesis and continued during shallow burial in Mn reducing environments (Fig. 16a). According to André et al. (2004) sedimentary dykes formed during the Late Jurassic. An extensive phase recorded in the Paris Basin and in the Dauphinois Basin and linked to the coeval opening of the Central Atlantic, the Piemont-Liguria Ocean and the North Sea was considered by these authors to explain the formation of sedimentary dykes. Fluids that percolated along these structural pathways allowed calcite precipitation in some coral geodes. This kind of geodic cementation is rare because of the scarcity of sedimentary dykes. During subaerial exposures of the basin margins at the Jurassic/Cretaceous boundary (LCU) and during the Aptian (LAU) meteoric water entered deep aquifers laterally from groundwater recharge zones. Fluids gradually became saturated with respect to calcite during their lateral and downward flow through host carbonates and with increasing chemical compaction away from basin margins. Cal1 and Cal2 precipitated from these mixed parent fluids during increasing burial with increasing reducing conditions and a low water/rock ratio. Oversaturation of fluids with respect to calcite and Cal2 precipitation were favoured by temperature increase with depth and by chemical compaction, the latter being more pronounced in facies with significant clay content. Chemical compaction favoured REE, Mg and Fe enrichment of fluids by release from clay material diluted in host rocks and concentrated in stylolites. In the Middle Jurassic, the first fracturing event which was prior to Cal1 was due to mechanical compaction or local synsedimentary extensional tectonism. In the Oxfordian, mechanical compaction is characterized by grain fracturing alone. This difference can be explained by the greater content of porous granular and early cemented facies in Middle Jurassic limestones than in Oxfordian limestones since the more porous facies strengthened by early cementation are more sensitive to crack propagation (Croizé et al., 2010).

According to Brigaud et al. (2009a) the first two generations of cements (named Cal1 and Cal2 in the present study) consist of more than 90% of the cementation volume in the Middle Jurassic limestones while in the Oxfordian they are restricted to grainstone facies of the *Calcaires de Dainville* member and the *Oolithe de Saucourt* member. Cal1 and Cal2 are never found in vugs and oolitic facies of the Middle Oxfordian except in the Calcaires de Dainville member. This discrepancy can be explained by the lateral distribution of sedimentary facies in both aquifers. Middle Jurassic carbonates consist in numerous granular facies (oncolitic, oolitic or bioclastic) with a grainstone texture. Their stratigraphic distribution constituted laterally continuous porous pathways from the recharge zones to the deeper parts of the basin and allowed a relatively substantial renewal of interstitial waters. By contrast, laterally continuous grainstone facies are rare in the Oxfordian. Fluids reached the deeper parts of the basin mainly through the *Calcaires de Dainville* and the *Oolithe de Saucourt* formations. Below, oolitic grainstones are not laterally continuous from the recharge zones to the deeper basin and geodes of coral neomorphism are entrapped in tight micritic sediments.

Telogenesis is characterized by several stages of fracturing. Cal3 and Cal4 calcite illustrate a continuum in the evolution of parent fluid chemistry. They indicate a gradual transition from reducing to oxidizing conditions. Cal3 marks the beginning of an opening in the system. The successive telogenetic phases of fracturing allowed circulations of sulphur- and fluorite-rich fluids. Cal4 in an Oxfordian geode has been dated to the Oligocene (Pisapia et al., 2011). However, the time span between Cal3 and Cal4 is unknown. F2 is probably linked to Pyrenean compression during the Late Cretaceous and early Cainozoic or to the Oligocene extension but the the flow(s) of parent fluid of Cal3 may be younger. Since they are prior to Cal4, Cal3 calcites are probably linked to the final stages of the Pyrenean compression or initial stages of Oligocene extension.

Precipitation of Cal4 probably occurred during the Oligocene but lasted at least until the Miocene period since Cal4 fills younger Alpine tension gashes. In the latter, Cal4 postdates Dol2 dolomite. The fluids were probably Mg enriched by horizontal stylolitic peaks during the Alpine phase. After removal of Mg from the fluid by Dol2, Cal4 precipitated in Alpine tension gashes. Cal3 and Cal4 constitute most or all the cements in the Middle Oxfordian vugs (geodes, moulds), and in minor laterally

discontinuous grainstone levels. In the Middle Jurassic limestone, CaI3 and CaI4 represent less than 10% of the total cement volume. In Oxfordian limestones telogenetic fracturing created new vertical flow pathways that permitted the fluid to reach coral neomorphism voids or interganular pores in grainstones. In the first stages, meteoric fluids were certainly in chemical disequilibrium with the host rock. These undersaturated fluids enhanced geodic voids by dissolution. Conversely, in the Middle Jurassic CaI3 and CaI4 fill only the residual porosity after the intensive cementation by CaI1 and CaI2. The southward decrease of the $\delta^{18}O$ values of CaI4 could be due to an increase in temperature. Such an increase was not due to deeper burial since during telogenesis the Alpine tectonic strain generated an uplift of the Vosges Massif and the southern part of the basin (Ziegler and Dèzes, 2007). The increase may be linked to the Rhine rifting during the Oligocene. However, such a regional increase in the geothermal gradient has not been documented until now. Another hypothesis is the southern input of freshwater from the Morvan Massif, the Burgundy High and/or the Vosges Massif. Northward, interactions with the host rocks may have slightly buffered the $\delta^{18}O$ of the parent fluid. Inputs may have occurred on the margins of the Vosges Massif exhumed during telogenesis. Present recharge zones of fluid in Middle and Upper Jurassic aquifers in the vicinity of the URL are from Oxfordian and Bajocian cuestas in the south-east (Linard et al., 2011). Waters in both aquifers are quite old and slow moving (Linard et al., 2011). The O and C isotope values of waters analysed by the Andra clearly indicate that water/rock interaction increases to the NW. The westward retreat of cuestas started during the Late Tertiary suggesting that parent fluids of CaI4 may in part have infiltrated from the borders of the Vosges Massif when aquifers cropped out further east. However, fluid flows were certainly slow or may have occurred in permeable deep aquifers such as the Triassic sandstones and fluids subsequently flowed upward by tectonic fractures since the substantial burial cementation in the Middle Jurassic and the predominance of muddy facies in the Oxfordian certainly prevented sizeable lateral fluid flows. The Hercynian Vittel Fault (Fig. 1) may also have favoured the upflow of deep meteoric fluids.

6 Conclusions

This study focused on similarities and differences between burial cementation in two Jurassic limestone series located below and above the thick clay formation in the eastern Paris Basin. Results

show that in the Eastern Paris Basin most of the cementation phases are linked to major geodynamic events. However burial and telogenesis cementation impacted the Middle and Upper Jurassic limestone Formations differently.

- The lateral recharge of deep aquifers by meteoric waters during Late Cimmerian and Late Aptian unconformities contributed to an intensive cementation in the dominantly grain-supported facies of the Middle Jurassic during burial. Jurassic to Cretaceous deep meteoric cementation was less developed in the Oxfordian mostly because of a dominance of mud-supported facies, the rare grain-supported intervals being as cemented as the Middle Jurassic ones. The fluid/rock ratio was low and reducing conditions were dominant due to the slow fluid migration and the low renewal of pore fluids in deep aquifers located several ten of kilometres away from the recharge areas. In this environment chemical compaction contributed to the final REE budget of calcite and contributed to the oversaturation of fluids with respect to calcite.

- Telogenetic fracturing during the Pyrenean and Alpine compressive phases and the Oligocene extensional phase opened up vertical fluid pathways responsible for (1) local dissolution by aggressive meteoric waters, and (2) the cementation in the Oxfordian geodes entrapped in mud-supported facies. Conversely, telogenetic flows did not create much secondary porosity in the Middle Jurassic, and the related cementation filled only the low residual pore spaces. This period corresponds to an opening of the system with the appearance of oxidizing conditions with a high fluid/rock ratio.

Acknowledgements:

This study is a part of Andra and TAPSS 2000 research program “Present and past transfers in a sedimentary aquifer – aquitard system: a 2000 meter deep drill-hole in the Mesozoic of the Paris Basin”, and was funded by GNR FORPRO. We thank the two anonymous reviewers who allowed improving the quality of the manuscript. We are grateful to R. Magott, S. Villard and J. Damato for their discussions about the carbonate paragenesis. We also thank C. Aurière for his kindness and his help in the Andra core shack.

References:

Aharonov, E., Katsman, R., 2009. Interaction between pressure solution and clays in stylolite development: insights from modelling. Amer. J. Sci. 309, 7, 607-632.

Allwood, A., Kamber, B., Walter, M., Burch, I., Kanik, I., 2010. Trace elemets record depositional history of an Early Archean stromatolitic carbonate platform. Chem. Geol. 270, 148-163.

Anderson, T., Arthur, M., 1983. Stables isotopes of oxygen and carbon and their application to sedimentologic and paleoenvironmental problems. in: Arthur, M. (Ed.), Stables Isotopes in Sedimentary Geology. SEPM Short Course No10, Tulsa, 439p.

André, G., Hibsch, C., Fourcade, S., Cathelineau, M., Buschaert, S., 2010. Chronology of Fracture Sealing under a Meteoric Fluid Environment: Microtectonic and Isotopic Evidence of Major Cainozoic Events in the Eastern Paris Basin (France). Tectonophysics, 490, 214-228.

André, G., Hibsch, C., Beaudoin, B., Carpentier, C., Fourcade, S., Cathelineau, M., Élion, P., 2004. Oxfordian sedimentary dykes: Tectonic and diagenetic implications for the eastern Paris basin. Bull. Soc. Géol. Fr. 175, 6, 595-605.

André, G., 2003. Caractérisation des déformations méso-cénozoïques et des circulations fluides dans l'Est du Bassin de Paris. Nancy, PhD thesis, Nancy University, 308 p.

Azmy, K., Brand, U., Sylvester, P., Gleeson, S., Logan, A., Bitner, M.A., 2011. Biogenic and abiogenic low-Mg calcite (bLMC and aLMC): Evaluation of seawater-REE composition, water masses and carbonate diagenesis. Chem. Geol. 280, 180-190.

Ballanca, A., Masetti, D., Neri, R., 1997. Rare earth elements in limestone/marlstone couplets from the Albian-Cenomanian Cismon section (Venetian region, northern Italy): assessing REE sensitivity to environmental changes. Chem. Geol. 141, 141-152.

Banner, J.L., Hanson, G., Meyers, W., 1988. Rare earth element and Nd isotopic variations in regionally extensive dolomite from the Burlington-Keokuk formation (Mississippian): Implications for REE mobility during carbonate diagenesis. J. Sed. Pet. 58, 3, 415-432.

Bathurst, R., 1987. Diagenetically enhanced bedding in argillaceous platform limestones – stratified cementation and selective compaction. Sedimentology, 34, 749–778.

Bau, M., Dulski, P., 1996. Distribution of yttrium and rare-earth elements in the Penge and Kuruma iron-formations, Transvaal Supergroup, South Africa. Precamb. Res. 79, 37-55.

Beier, J.A., 1985. Diagenesis of Quaternary Bahamian beachrock: petrographic and isotopic evidence. J. Sed. Pet. 55, 5, 755–761.

Bengtsson, A., Lindegren, M., Sjöberg, S., Persson, P., 2007. Dissolution, adsorption and phase transformation in the fluorapatite-goethite system. Applied Geochemistry 22, 2016 – 2028.

Blaise, T., 2012. Histoire thermique et interactions fluides-roches dans l'Est du Bassin de Paris. PhD Thesis, Lorraine University, 350 pp.

Brand, U., Veizer, J., 1980. Chemical diagenesis of a multicomponent carbonate system – 1: trace elements. J. Sed. Pet. 50, 4, 1219-1236.

Braun, J. J., Pagel, M., Muller, J. P., Bilong, P., Michard, A., Guillet, B., 1990. Cerium anomalies in lateritic profiles. Geochim. Cosmochim. Acta, 54, 781–795.

Brigaud, B., Vincent, B., Durlet, C., Deconinck, J.F., Blanc, P., Trouiller, A., 2010. Acoustic Properties of Ancient Shallow-Marine Carbonates: Effects of Depositional Environments and Diagenetic Processes (Middle Jurassic, Paris Basin, France). J. Sed. Res., 80, 9, 791-807.

Brigaud, B., 2009. Influence du contexte sédimentaire et de la diagenèse sur les propriétés pétrophysiques du Dogger calcaire de l'est du Bassin de Paris. PhD Thesis, University of Bourgogne, Dijon, France, 340 p.

Brigaud, B., Durlet, C., Deconinck, J.F., Vincent, B., Thierry, J., Trouiller, A., 2009a. The Origin and Timing of Multiphase Cementation in Carbonates: Impact of Regional Scale Geodynamic Events on the Middle Jurassic Limestones Diagenesis (Paris Basin, France). Sed. Geol. 222, 161-180.

Brigaud, B., Durlet, C., Deconinck, J.F., Vincent, B., Pucéat, E., Thierry, J., Trouiller, A., 2009b. Facies and climate/environmental changes recorded on a carbonate ramp: A sedimentological and geochemical approach on Middle Jurassic carbonates (Paris Basin, France). Sed. Geol. 222, 181-206.

Buschaert, S., Fourcade, S., Cathelineau, M., Deloule, E., Martineau, F., Ougougdal, A.M., Trouiller, A., 2004. Widespread Cementation Induced by Inflow of Continental Water in the Eastern Part of the Paris Basin: O and C Isotopic Study of Carbonate Cements. Appl. Geoch. 19, 1201-1215.

Calvet, F., Cabrera, M.C., Carracedo, J.C., Mangas, J., Pérez-Torrado, F.J., Recio, C., Trave, A., 2003. Beachrocks from the island of La Palma (Canary Islands, Spain). Mar. Geol. 197, 75–93

Carpentier, C., Lathuilière, B., Ferry, S., 2010. Sequential and Climatic Framework of the Growth and Demise of a Carbonate Platform: Implications for the Peritidal Cycles (Late Jurassic, North-Eastern France). Sedimentology, 57, 985-1020.

Carpentier, C., Lathuilière, B., Ferry, S., Sausse, J., 2007. Sequence Stratigraphy and Tectonosedimentary History of the Upper Jurassic of the Eastern Paris Basin (Lower and Middle Oxfordian, Northeastern France). Sed. Geol. 197, 235-266.

Chaïrat, C., Schott, J., Oelkers, E.H., Lartigue, J.E., Harouiya, N., 2007. Kinetics and mechanism of natural fluorapatite dissolution at 25 ℃ and pH fr om 3 to 12. Geochim. Cosmochim. Acta 71, 5901 – 5912.

Collin, P.Y., Courville, P., 2006. Sedimentation and palaeogeography of the eastern part of the Paris Basin (France) at the Middle–Upper Jurassic boundary. C. R. Geoscience, 338, 824–833

Collin, P.Y., Courville, P., Loreau, J.P., Marchand, D., Thierry, J., 1999. Séries condensées et indice de préservation d'unité biostratigraphique : exemple de l'ennoiement de la plate-forme nord-bourguignonne (France) au Callovo-Oxfordien. C.R. Acad. Sci. Paris, 328, 105-111.

Coulon, M., Frizon de Lamotte, D., 1988. Les extensions cénozoïques dans l'Est du Bassin de Paris : mise en évidence et interprétation. C.R. Acad. Sci. Paris, 307, 1113-1119.

Croizé, D., Ehrenberg, S., Bjørlykke, K., Renard, F., Jahren, J., 2010. petrophysical properties of bioclastic platform carbonates: implications for porosity controls during burial. Mar. Petrol. Geol. 27, 1765-1774.

Demars, C., Pagel, M., 1994. Paléotempératures et paléosalinités dans les grès du Keuper du Bassin de Paris: inclusions fluides dans les minéraux authigènes. C.R. Acad. Sci. Paris. 319, II, 427-434.

De-Graciansky, D., Jacquin, T., 2003. Evolution des structures et de la paléogéographie au passage Lias-Dogger dans le Bassin de Paris d'après les données de la subsurface. Bull. Soc. Géol. Fr. 174, 1, 3-17.

Denniston, R., Shearer, C., Layne, G., Vaniman, D., 1997. SIMS analyses of minor and trace element distributions in fracture calcite from Yucca mountain, Nevada, USA. Geochim. Cosmochim. Acta, 61, 9, 1803-1818.

Dickson, J., 1965. A modified staining technique for carbonates in thin section. Nature, 4971, 587.

Durlet, C., Lathuiliere, B., Aycard, M., 2001. Reef geometries and facies in Bajocian limestones of the Burgundy High (France): Environmental and sequence stratigraphy interpretations. Eclog. Geol. Helv. 94, 1, 1-11.

Durlet, C., Thierry, J., 2000. Aalenian and Bajocian depositional sequences on the Burgundy High (France). Bull. Soc. Geol. Fr. 171, 3, 327-339.

Durlet, C., Thierry, J., Floquet, M., 1997. Tectonique synsédimentaire distensive dans les calcaires aaléno-bajociens du Seuil de Bourgogne (France) C.R. Acad. Sci. Fr. Paris, 324, 12, 1001-1008.

Durlet, C., Loreau, J.P., 1996. Séquence diagénétique intrinsèque des surfaces durcies : mise en évidence de surface d'émersion et de leur ablation marine. Exemple de la plate-forme bourguignonne, Bajocien (France). C. R. Acad. Sci. Fr. Paris, 323, (2a), 389-396.

Durlet, C., 1996. Apport de la diagenèse des discontinuités à l'interprétation paléo-environnementale et séquentielle d'une plate-forme carbonatée. Exemple des Calcaires à entroques du Seuil de Bourgogne (Aalénien-Bajocien). PhD Thesis, Bourgogne University, France, 444 pp.

Elderfield, H., 1988. The oceanic chemistry of rare-earth elements. Philos. Trans. R. Soc. London, 325, 105-126.

Espitalié, J., Marqis, F., Sage, L., Barsony, I., 1987. Géochimie organique du Bassin de Paris. Oil & Gas Science and Technology, Revue de l'IFP, 42, 271-302.

Gaucher, E., Robelin, C., Matray, J.M., Négrel, G., Gros, Y., Heitz, J.F., Vinsot, A., Rebours, H., Cassagnabère, A., Bouchet, A., 2004. ANDRA underground research laboratory: interpretation of the mineralogical and geochemical data acquired in the Callovian–Oxfordian formation by investigative drilling. Phys. Chem. Earth, 29, 55–77.

Granier, B., Staffelbach, C., 2009. Quick look cathodoluminescence analyses and their impact on the interpretation of carbonate reservoirs. Case study of mid-Jurassic oolitic reservoirs in the Paris Basin. Notebooks on Geology, CG2009_A06.

Guillocheau, F., Robin, C., Allemand, P., Bourquin, S., Brault, N., Dromart, G., Friedenberg, R., Garcia, J.P., Gaulier, J.M., Gaumet, F., Grosdoy, B., Hanot, F., Le Strat, P., Mettraux, M., Nalpas, T., Prijac, C., Rigollet, C., Serrano, O., Grandjean, G., 2000. Meso-Cenozoic Geodynamic Evolution of the Paris Basin: 3d Stratigraphic Constraints. Geodin. Acta, 13, 189-246.

Haley, B., Klinkhammer, G., McManus, J., 2004. Rare earth elements in pore waters of marine sediments. Geochim. Cosmochim. Acta, 68, 6, 1265-1279.

Hendry, J.P., 2002. Geochemical trends and palaeohydrological significance of shallow burial calcite and ankerite cements in Middle Jurassic strata on the East Midlands Shelf (onshore UK). Sed. Geol. 151, 149-176.

Heydari, E., 2003. Meteoric versus burial control on porosity evolution of the Smackover Formation. AAPG Bull., 87, 11, 1779-1797.

Hillgartner, H., Dupraz, C., Hug, W. 2001. Microbially induced cementation of carbonate sands: are micritic meniscus cements good indicators of vadose diagenesis? Sedimentology, 48, 117-131.

Holail, H., Rashed, M., 1992. Stable isotopic composition of carbonate-cemented recent beachrock along the Mediterranean and Red Sea Coasts of Egypt. Mar. Geol. 106, 141–148.

Jacquin, T., Dardeau, G., Durlet, C., De Graciansky, P.C., Hantzpergue, P., 1998. The North Sea Cycle: An Overview of 2nd-Order Transgressive/Regressive Faciès Cycles in Western Europe, in: De Graciansky, P.C., Hardenbol, J., Jacquin, T., Vail, P.R. (Eds.) Mesozoic and Cenozoic Sequence Stratigraphy of European Bassins. SEPM Spec. Pub. n°60, Tulsa, 445-466.

Javaux, C., 1992. La plate-forme parisienne et bourguignonne au Bathonien terminal et au Callovien—Dynamique sédimentaire, séquentielle et diagénétique, Place et création des réservoirs potentiels, 16. Mémoires géologiques de l'Université de Dijon, Dijon. 342 pp.

Kobluk, D.R., Risk, M.J., 1977. Micritization and Carbonate-Grain Binding by Endolithic Algae. AAPG Bull. 61, 1069-1082.

Lacombe, O., Obert, D., 2000. Héritage structural et deformation des couverture : plissement et fracturation tertiaires dans l'Ouest du bassin de Paris. C. R. Acad. Sci. Paris, 330, 793–798.

Lathuilière, B., 2008. Eastern Paris Basin, In: Mc Cann, T. (Ed.) The geology of central Europe. Vol. 2: Mesozoic and Cenozoic. Geol. Soc. London, London, p. 854-858.

Lecuyer, C., Picard, S., Garcia, J.P., Sheppard, S.M.F., Grandjean, P., Dromart, G., 2003. Thermal evolution of Tethyan surface waters during the Middle-Late Jurassic: Evidence from δ18O values of marine fish teeth. Palaeoceanography, 8, 3, 21-1

Lefort, A., Lathuilière, B., Carpentier, C., Huault, V., 2011. Microfossil assemblages and relative sea-level fluctuations in a lagoon at the Oxfordian/Kimmeridgian boundary (Upper Jurassic) in the eastern part of the Paris Basin. Facies, 57, 4, 649-662.

Leroux, J., 1980. Jurassique moyen, in Mégnien, C., Mégnien, F. (Eds.) Synthèse géologique du Bassin de Paris. Vol. 1 Stratigraphie et paléogéographie, Mem. BRGM n°101, p. 160-167.

Leybourne, M., Goodfellow, W., Boyle, D., Hall, G., 2000. Rapid development of negative Ce anomalies in surface waters and contrasting REE patterns in groundwaters associated with Zn-Pb massive sulphide deposits. Appl. Geoch., 15, 695-723.

Linard, Y., Vinsot, A., Vincent, B., Delay, J., Wechner, S., De La Vaissière, R., Scholz, E., Garry, B., Lundy, M., Cruchaudet, M., Dewonck, S., Vigneron, G., 2011. Water flow in the Oxfordian and Dogger limestone around the Meuse/Haute-Marne Underground Research Laboratory. Phys. Chem. Earth, 36, 1450–1468.

Longerich, H.P., Jackson, S.E., Günther, D., 1996. Laser ablation inductively coupled plasma mass spectrometric transient signal data acquisition and analyte concentration calculation. J. Anal. Atom. Spectrom. 11, 899-904.

Machel, H., 1999. Effects of groundwater flow on mineral diagenesis, with emphasis on carbonate aquifers. Hydrogeol. Journal, 7, 94-107.

Malartre, F., Dagallier, G., Lathuilière, B., Leroux, J., 1999. Modalités d'installation et de développement de la plate-forme carbonatée du Bajocien inférieur de Lorraine (NE France). ASF publ. *n°33* , Nancy, *p. 221.*

Malfilatre, C., Boulvais, P., Dabard, M.P., Bourquin, S., Hallot, E., Pallix, D. Gapais, D., 2012. Petrographical and geochemical characterization of Comblanchien limestone (Bourgogne, France): A fingerprint of the building stone provenance. C.R.Geosc.Paris, 344, 1, 14-24

Mangold, C., Poirot, E., Lathuilière, B., Leroux, J., 1994. Biochronologie du Bajocien supérieur et du Bathonien de Lorraine. Geobios spec. Mem. 17, p.343-349.

Megnien, F., 1980. Synthèse géologique du Bassin de Paris. Vol. III Lexique des noms de formation, BRGM Mem. 103, Orléans, pp. 467.

Melim, L.A., Westphal, H., Swart, P.K., Eberli, G.P., Munnecke, A., 2002. Questioning carbonate diagenetic paradigms: evidence from the Neogene of the Bahamas. Mar. Geol., 185, 27-53.

Moore, C.H., 2001. Carbonate Reservoirs: Porosity Evolution and Diagenesis in a Sequence stratigraphic Framework. Developments in sedimentology, 55, Elsevier, New-York, 460 pp.

Mortimore, R., Pomerol, B., 1997. Upper Cretaceous tectonic phases and end Cretaceous inversion in the Chalk of the Anglo-Paris Basin. *Proceedings of the Geologist's Association,* 108, 231- 255.

Murray, R., Buchholtz ten Brink, M., Jones, D., Gerlach, D., Price Russ III, G., 1990. Rare earth elements as indicator of different marine depositional environments in chert and shale. Geology, 18, 268-271.

Nesbitt, B., Muehlenbachs, K., 1997. Paleo-hydrology of Late Proterozoic units of southeastern Canadian Cordillera. Amer. J. Sci. 297, 359-392.

Nothdurft, L., Webb, G., Kamber, B., 2004. Rare earth elements geochemistry of Late Devonian carbonates, Canning Basin, Western Australia: Confirmation of a seawater REE proxy in ancient limestones. Geochim. Cosmochim. Acta, 68, 2, 263-283.

Olivier, N., Boyet, M., 2006. Rare earth trace elements of microbialites in Upper Jurassic coral- and sponge-microbialite reefs. Chem. Geol. 230, 105-123.

O'Neil, J.R., Claytonm, R.N., Mayeda, T.K., 1969. Oxygen isotope fractionation in divalent metal carbonates. J. Chem. Phys. 51, 5547–5558.

Palmer, T., Hudson, J., Wilson, M., 1988. Palaeoecolgical evidence for early aragonitic dissolution in ancient calcite seas. Nature, 335, 809-810.

Palmer, R.M., 1985. Rare earth elements in foraminifera tests. Earth Planet. Sc. Lett. 73, 285-298.

Pattan, J., Pearce, N., Mislankar, P., 2005. Constraints in using Cerium anomaly of bulk sediments as an indicator of paleo bottom water redox environment : A case study from the Central Indian Ocean Basin. Chem. Geol. 221, 260-278.

Pellenard, P., Deconinck, J.F., Huff, W.D., Thierry, J., Marchand, D., Fortwengler, D., Trouiller, A., 2003. Characterization and correlation of Upper Jurassic (Oxfordian) bentonite deposits in the Paris Basin and the Subalpine Basin, France. Sedimentology, 50, 1035-1060.

Pellenard, P., Deconinck, J.F., Marchand, D., Thierry, J., Fortwengler, D., Vigneron, G., 1999. Eustatic and volcanic influence during Middle Callovian to Middle Oxfordian clay sedimentation in the eastern part of the Paris Basin. C.R.Acad.Sci.Paris. 328, 807-813.

Pinti, D., Marty, B., 1995. Noble gases in crude oils from the Paris Basin, France: Implications for the origin of fluids and constraints on oil-water-gas interactions. Geochim. Cosmochim. Acta, 59, 16, 3389-3404

Pisapia C., Deschamps P., Hamelin B., Battani A., Buschaert S., David J., 2011. U/Pb dating of geodic calcite: A tool for paleohydrological reconstructions. Goldschmidt international conference, Prague, abstract book, p. 1647.

Purser, B.H., 1989. Plates-formes carbonatées : exemple du Jurassique moyen du Bassin de Paris, dynamique et méthodes d'étude des bassins sédimentaires. Technip, Paris, 260 pp.

Purser, B.H., 1980. Sédimentation et diagenèse des carbonates néritiques récents, Tome 1. Technip, Paris, 366 pp.

Rude, P.D., Aller, R.C., 1991. Fluorine mobility during early diagenesis of carbonate sediment: An indicator of mineral transformations. Geochim. Cosmochim. Acta, 55, 2491 – 2509.

Sandberg, P.A., 1983. An oscillating trend in Phanerozoic non-skeletal carbonate mineralogy. Nature, 305, 19–22.

Scherer, M., Seitz, H., 1980. Rare-earth elements distribution in Holocene and Pleistocene corals and their redistribution during diagenesis. Chem. Geol., 28, 279-289.

Schieber, J., 1988. Redistribution of rare earth elements during diagenesis of carbonate rocks from the Mid-Proterozoic Newland formation, Montana, U.S.A. Chem. Geol., 69, 111-126.

Shields, G., Stille, P., 2001. Diagenetic constraints on the use of cerium anomalies as paleoseawater redox proxies: an isotopic and REE study of Cambrian phosphorites. Chem. Geol. 175, 29-48.

Sterpenich, J., Sausse, J., Pironon, J., Géhin, A., Hubert, G., Perfetti, E., Grgic, D., 2009. Experimental ageing of oolitic limestones under CO_2 storage conditions. Petrographical and chemical evidence. Chem. Geol., 265, 99-112.

Taylor, S., McLennan, S., 1985. The continental crust: its composition and evolution. Blackwell, Oxford, p.311.

Thiry-Bastien, P., 2002. Stratigraphie séquentielle des calcaires bajociens de l'est de la France (Jura-Bassin de Paris). PhD Thesis, Université Claude Bernard, Lyon, France, 409 p.

Tribble, J.S., Arvidson, R.S., Lane, M., MacKenzie, F.T., 1995. Crystal chemistry, and thermodynamic and kinetic properties of calcite, dolomite, apatite, and biogenic silica: applications to petrologic problems. Sed. Geol. 95, 11 – 37.

Uysal, I., Zhao, J.X., Golding, S., Lawrence, M., Glikson, M., Collerson, K., 2007. Sm-Nd dating and rare-earth element tracing of calcite : implications for fluid-flow events in the Bowen Basin, Australia. Chem. Geol., 238, 63-71.

Vandycke, S., 2002. Palaeostress records in Cretaceous formations in NW Europe: extensional and strike-slip events in relationships with Cretaceous–Tertiary inversion tectonics. Tectonophysics, 357 (1–4), 119–136.

Vincent, B., Emmanuel, L., Houel, P., Loreau, J.P., 2007. Geodynamic Control on Carbonate Diagenesis: Petrographic and Isotopic Investigation of the Upper Jurassic Formations of the Paris Basin (France). Sed. Geol., 197, 267-289.

Vincent, B., 2001. Sédimentologie et géochimie de la diagenèse des carbonates. Application au Malm de la bordure Est du Bassin de Paris. PhD Thesis, Université de Bourgogne, Dijon, France, 308 pp.

Webb, G., Kamber, B., 2000. Rare earth elements in Holocene reefal microbialites : A new seawater proxy. Geochim. Cosmochim. Acta, 64, 9, 1557-1565.

Webb, G., Nothdurft, L., Kamber, B., Kloprogge, J., Zhao, J.X., 2009. Rare earth element geochemistry of scleractinian coral skeleton during meteoric diagenesis: a sequence through neomorphism of aragonite to calcite. Sedimentology, 56, 1433-1463.

Webb, G., Jell, J., Baker, J., 1999 Cryptic intertidal microbialites in beachrock, Heron Island, Great Barrier Reef: implications for the origin of microcrystalline beachrock cement. Sed. Geol., 126, 317–334.

Worden, R., Mattray, J., 1995. Cross formational flow in the Paris Basin. Basin Res., 7, 53-66

Wyndham, T., McCulloch, M., McManus, J., 2004. Rare earth elements in pore waters of marine sediments. Geochim. Cosmochim. Acta, 68, 6, 1265-1279.

Ziegler, P, A, Dèzes, P, 2007. Cenozoic Uplift of Variscan Massifs in the Alpine Foreland: Timing and Controlling Mechanisms. Global Planet. Change, 58, 237-269.

Zhu, Y., Zhang, X., Chen, Y., Xie, Q., Lan, J., Qian, M., He, N., 2009. A comparative study on the dissolution and solubility of hydroxylapatite and fluorapatite at 25 ℃ and 45 ℃. Chem. Geol. 268, 89 – 96.

Table caption:

Table 1: Relative abundance of diagenetic features in Middle and Late Jurassic aquifers.

Table 2: Comparative table of cement characteristics described in the litterature and results of the present study.

Figures captions:

Figure 1: Location map of the studied outcrops and cored wells.

Figure 2: Simplified Jurassic and Cretaceous stratigraphic column of the Paris Basin with main argillaceous formation surrounding or intercalated with Jurassic aquifers (modified from Guillocheau et al., 2000; Megnien, 1980; Thicknesses not to scale)

Figure 3: Middle Jurassic lithostratigraphy of the eastern Paris Basin (modified from Brigaud et al., 2009b; Lathuilière, 2008; Le Roux, 1980, Malartre et al., 1999; Mangold et al., 1994; Thiry-Bastien, 2002)

Figure 4: Oxfordian lithostratigraphy of the eastern Paris Basin (modified from Carpentier et al., 2007; 2010)

Figure 5: Diagenetic stratigraphy of Middle and Upper Jurassic aquifers in relation to major discontinuities, burial and exhumation periods of the eastern Paris Basin

Figure 6: Main petrographic characteristics of eogenetic and early mesogenetic features. (a) Early marine fibrous cements (EIRC) on the edges of an echinoid clast (E) affected by destructive micritization (Mf). Under cathodoluminescence the growth of the early fibrous cements is inhibited by the growth of the early stage of a syntaxial cement (Sy) constituted by Cal0, Cal1 and Cal2. The geometrical relationship between cements indicates that the Cal0 syntaxial zone predates the EIRC (*Dalle d'Etain* Fm., A901 drill core). (b) Pyrite (Py1) and calcite cements (EIRC: Early inclusion-rich cements, Cal0: Scalenohedral fringe of early inclusion-poor calcite, Cal1 and 2: Calcite 1 and 2

cements) in an ooid grainstone (*Oolithe miliaire*, EST 210 core, Middle Jurasssic). (c) A non-luminescent meniscus cement (Me), equivalent to the Cal0 inclusion-poor calcite in oolitic grainstone of the *Calcaires de Dainville* Mbr (Pagny-sur-Meuse quarry). (d) Pendant fibrous cement (Mc) (*Oolithe de Doulaincourt* Fm.). (e) Non-luminescent early Cal0 blocky calcite surrounding micritic ooids (Top of the *Calcaires Crayeux de Maxey* Mbr., EST 205 drill core). (f) Inclusion-rich, non-ferroan neomorphic calcite (Nc) in a geode filled by ferroan Cal2 blocky calcite displaying a violet colour after staining (*Calcaires à polypiers supérieurs*, Malancourt quarry). (g) F1 fractures filled by non-ferroan Cal1 calcite and ferroan Cal2 calcite (*Oolithe de Doncourt* Fm., A901 drill core). (h) Microspar dyke showing a first infill by non-ferroan spar (Ec) prior to microcrystalline calcite (Ms). Note the occurrence of micrite intraclasts (Mc) in spar and the fracture edge parallel micritic laminations in the microspar (*Calcaires crayeux de Maxey* Mbr., Sorcy quarry).

Figure 7: Main petrological characteristics of mesogenetic and early telogenetic cements. (a) Cal1 calcite showing a bright orange luminescence and a zoning pattern under CL (*Dalle d'Etain* Fm., Thin-le-Moutier quarry). (b) Neomorphic calcite (Nc) in a geode overlain by Cal1 showing orange luminescence. The younger Cal2 calcite displays a dull dark brown luminescence and fills the residual porosity (*Calcaires à polypiers supérieurs*, Jaumont quarry). (c) Dol1 and Dol2 dolomite in micritic limestone under CL. Note the euhedral luminescent core subzone of Dol1. A relatively large non-luminescent rim with a thin, bright orange, external fringe is visible. Bright orange luminescence of Dol2 can be observed (*Calcaires de Chaumont*, EST 433 core). (d) Dol1 dolomite in insoluble clayed material within a stratiform stylolite under CL (*Calcaires de Dainville* Mbr., EST 204 drill core). (e) Ferroan Cal2 and non-ferroan Cal3 calcite in intergranular porosity. F2 fractures filled by Cal3 crosscut early fibrous cements (EIRC) and Cal2; OS = oyster shell (*Dalle d'Etain* Fm, A901 drill core). (f) Previous thin section under CL. The Cal2 calcite shows dull brown luminescence without zoning while C3 calcites are characterized by bright orange luminescence and zoning. Note F2 fractures crosscutting Cal2 calcite. (g) Ferroan Cal2 calcite in intergranular porosity in an Upper Oxfordian grainstone (*Oolithe de Saucourt inférieure* Mbr., Pagny-sur-Meuse quarry). (h) F2 fractures cutting across Cal2 calcite. F2 are connected with intergranular Cal3 calcite. The lack of Cal3 where pyrite (Py2) is in contact with Cal2 suggests that Py2 is prior to Cal3 (*Dalle d'Etain* Fm., A901 drill core). (i) After the transformation of coral aragonite in neomorphic calcite (Nc) the geode was filled by Cal1,

Cal2 and euhedral quartz (Qtz) (*Calcaires à polypiers inférieurs* Fm., Malancourt quarry). (j) Chalcedony (Cy) replacement of echinoid spine. Chalcedony is crosscut by F3 fractures filled by Cal4 (*Oolithe de Jaumont* Fm., Jaumont quarry). (k) F2 fractures filled by Cal3 calcite. Fractures fed the spaces generated by oolite desquamation (same thin-section under CL on the left and in natural light after Dickson coloration on the right, *Dalle d'Etain* Fm., A901 drill core). (l) F2 fractures filled by Cal3 cutting across F1 filled by Cal2 (*Calcaires à polypiers inférieurs* Fm., Bazoilles-sur-Meuse quarry). (m) F3 Fracture slightly or not affected by vertical peaks of stylolites. The shift of the fracture is largely lower than the shift generated by the stylolite suggesting that F3 formed only during the last stages of burial solution pressure (*Calcaires à polypiers inférieurs* Fm., A901 drill core).

Figure 8: Main telogenetic features. (a) Cal3 calcite in Oxfordian limestones, characterized by orange luminescence and faint zoning under CL (*Calcaires de Dainville* Mbr., EST 204 drill core). (b) Fluorine Fl1 replacing matrix, Dol1 and Cal2 calcite (*Calcaires à polypiers inférieurs* Fm., Malancourt quarry). (c) Replacement of carbonate grains and early marine cements by fluorite (Fl1a). The last stages of Fl1 growth consist of euhedral crystals in the intergranular pores (Fl1e). F3 filled by Cal4 and remobilized fluorite Fl2 crosscut Fl1. (*Calcaires crayeux de Gudmont* Mbr., EST 204 drill core). (d) Compressive stylolite (S2) crosscutting a fluorine vein of Fl1. Dol2 is associated with Cal4 in relay zones (arrows). Remobilized fluorite Fl2 is also locally present in relay zones (*Calcaires crayeux de Gudmont* Mbr. EST 204 drill core). (e) Fluorite Fl1 posterior to neomorphic calcite and prior to Cal4 in a coral dissolution geode in the Middle Jurassic (*Calcaires à polypiers supérieurs* Fm. Jaumont quarry). (f) Cal4 calcite in an F3 fracture crosscutting Dol1 and Cal2. (*Calcaires compacts de Neufchâteau* Fm., Bazoilles-sur-Meuse quarry). (g) Dol1, Dol2 and Cal4 cements in ooid (oo) grainstone with a relatively wide, non-luminescent zone with a thin, bright orange, external fringe is observed. Note the bright orange luminescence of Dol2, Cal4 cement with dull brown luminescence (*Calcaires de Chaumont* Fm., EST 210 drill core). (h) F2 fracture filled by Dol2 dolomite on edges and Cal4 calcite (*Calcaires coralliens d'Euville* Fm., EST 205 drill core). (i) Dol2 dolomite and Cal4 in a coral dissolution geode (*Calcaires coralliens d'Euville* Mbr., EST 204 drill core). (j) Cal4 and Dol2 are non-ferroan and exclusive in most of the Oxfordian geodes (*Calcaires coralliens d'Euville* Mbr., EST 204 drill core).

Figure 9: Orientations of main fracturing events in the Middle Jurassic and Oxfordian limestones of the eastern Paris Basin. Despite a slight predominance of NE–SW directions, Fd1 fractures display a wide range of directions. The low number of values provide no evidence of a preferential direction of Fd2. Conversely, Fd3 fractures indicate a preferential 150°N orientation. Oxfordian sedimentary dykes show a preferential 20°N direction except in the Du gny-sur-Meuse quarry where 80°N and 140°N directions predominate. Fo2 and Fo3 show main directions of about 20°N and 140°N respectively.

Figure 10: Comparison of $\delta^{18}O$ and $\delta^{13}C$ cross-plots of Middle Jurassic and Oxfordian blocky cements between previous works and the present study. (a) Stable oxygen and carbon isotopes of main cements analysed in the present study. Note the $\delta^{13}C$ enrichment of cements in Oxfordian limestones compared with the Middle Jurassic ones and the gradual decline in $\delta^{18}O$ values from Cal1 to Cal4 cements; (b) Published isotope data from blocky calcite cements from the Middle and Upper Jurassic limestones in interganular pores and geodes. Note the lack of equivalent to Middle Jurassic Bc2 calcite of Brigaud et al. (2009a) in Oxfordian limestones; (c) Stable oxygen and carbon isotopes of calcite in sedimentary dykes, Pyrenean and Alpine tension gashes and in Oligocene faults of the Gondrecourt graben.

Figure 11: Medium REE patterns with envelopes of values and trace element contents of Middle Jurassic and Oxfordian blocky cements and host rocks. Cal2 calcite show a flat REE-enriched pattern compared with the pattern for Oxfordian sea water published by Olivier and Boyet (2006). These cements lack any apparent Ce anomaly and are characterized by high Mg and Fe contents. Patterns reflect REE patterns of host limestones with a terrigenous contribution (Al enrichment). Cal3 shows alternating REE-enriched and LREE-depleted patterns with an apparent Ce anomaly. Cal4 and Oxfordian fluorite show a sea water-like pattern. However, Middle Jurassic calcites are REE-enriched compared with Oxfordian calcites. These patterns reflect composition of host rocks when older blocky cements are absent. The first generation of dolomite (Dol1) displays a flat pattern without any apparent Ce anomaly while the second generation (Dol2) exhibits a slightly REE-enriched sea water pattern with a Ce anomaly.

Figure 12: Burial history of the Jurassic from the eastern Paris Basin

Fig 13: Fractionation diagram from which it is possible to estimate the parent fluids of blocky calcites according to precipitation temperatures and the $\delta^{18}O$ composition of cements

Figure 14: (Ce/Ce*) vs (Pr/Pr*) diagram used to discriminate La and Ce anomalies (after Bau and Dulski, 1996). The Ce anomaly increases from older (Cal2) to younger blocky cements (Cal4). The same evolution is visible between mesogenetic (Dol1) and telogenetic (Dol2) dolomites. The Ce anomaly is lacking in host rocks where Cal2 precipitated and more pronounced in host rocks where Cal2 is absent.

Figure 15: Distribution of stylolites, early surfaces of subaerial exposure, textures and Cal2 cements along the EST 204 drill core in Oxfordian limestones. Note that Cal2 is not correlated with early exposures but a correlation occurs between the intensity of chemical compaction (stylolites and microstylolites), texture and Cal2. Where chemical compaction is intense, Cal2 is observed only in interganular porosity of grainstone facies and is absent in facies with matrix. Conversely, grainstone facies little affected by chemical compaction are devoid of Cal2.

Figure 16: General diagenetic model for both Middle Jurassic and Oxfordian aquifers and connections with main fluid circulation events in the eastern Paris Basin. After early cementation, neomorphism of coral aragonite and formation of sedimentary dykes occurred during early burial. During the early Cretaceous, lateral reload of deep aquifers with meteoric waters was possible during uplift of the basin margins (LCU and LAU). Precipitation of Cal1 and Cal2 calcite from a mixed meteoric-marine parent fluid occurred under reducing conditions probably during maximum burial (Upper Cretaceous). Chemical compaction presumably largely contributed to Dol1 precipitation, to the REE budget of Cal2 and probably to the oversaturation of fluid with respect to calcite. Lateral permeability of grainstone facies in the Middle Jurassic permitted a substantial advent of fluids in the deep parts of the aquifer and the precipitation of Cal2. Conversely, the micritic lagoonal facies in most Oxfordian limestones prevented intensive cementation during the Cretaceous. First telogenetic fracturing formed new vertical fluid pathways and allowed Cal3 calcites to precipitate in Oxfordian geodes during the transition from reducing to oxidizing conditions. From the Oligocene to the present, the last fracturing

events favoured vertical circulations of meteoric fluids and precipitation of Cal4 calcite which filled most of the geode porosity in Oxfordian limestones. Dol2 is linked to the last Alpine compressive event and may have originated in horizontal stylolitic peaks.

	Middle Jurassic	Late Jurassic
Early cements	Abundant	Rare
Pyrite 1 (Py1)	Rare	Absent
Mechanical compaction and F1 fractures	Common	Rare
Microspar fractures	Rare	Common
Calcite 1 (Cal1)	Common	Absent
Chemical compaction and stylolites 1 (Ccs1)	Common	Common
Dolomite 1 (Dol1)	Common in the vicinity of stylolites	Common in the vicinity of stylolites
Calcite 2 (Cal2)	Abundant	Absent in geodes
		Common in grainstones
Quartz 1 (Qz1)	Rare	Rare
F2 fractures	Rare	Rare
Pyrite 2 (Py2)	Rare	Rare
Calcite 3 (Cal3)	Common	Common
Fluorite 1 (Fl1)	Rare	Rare
F3 fractures	Rare	Rare
Stylolites 2 (S2)	Common	Common
Dolomite 2 (Dol2)	Rare	Rare
Fluorite 2 (Fl2)	Rare	Rare
Calcite 4 (Cal4)	Rare	Abundant in geodes
		Rare in grainstones

Brigaud et al (2009) Middle Jurassic							Vincent et al (2009) Oxfordian							This study (Middle Jurassic + Oxfordian)								André et al (2004) Sedimentary dykes and Tertiary Tension gashes	Buschaert et al (2004) Oligocene faults + Oxfordian geodes		
	Lu.	Zo.	Por.	Frac.	Fe	$\delta^{18}O$ (V-PDB)		Lu.	Zo.	Por.	Frac.	Fe	$\delta^{18}O$ (V-PDB)		Lu.	Zo.	Por.	Frac.	Fe	$\delta^{18}O$ (V-PDB)		$\delta^{18}O$ (V-PDB)	Lu.	Zo.	$\delta^{18}O$ (V-PDB)
														Md1						Mid.Oxf -6.7‰ ±0.3		Mid.Oxf. -6.6‰ ±0.3			
Bc1	Bright	Y	Y	N	N	-4.9‰ ±0.9								***Cal1***	Bright	Y	Y	Y	N	Dogger -5.0‰ ±0.9					
Bc2	Dull	N	Y	Y	Y	-6.7‰ ±0.7								***Cal2***	Dull	N	Y	Y	Y	Dogger -7.3‰ ±0.4 Malm -7.2‰ ±0.1	Average -7.3‰ ±0.4				
							Bc1 + Bc2	Bright	Y	Y	N	N	-8.6‰ ±1.4 -8.3‰ ±1.5	***Cal3***	Bright	Y	Y	Y Dog N Oxf	N	Dogger -8.3‰ ±0.8 Malm -7.8‰ ±0.2	Average -8.0‰ ±0.6				
Bc3	Dull	Y	Y	N	N	-9.9‰ ±0.9	***Bc3***	Dull	Y	Y	Y	N	-9.3‰ ±1.3	***Cal4***	Dull	Y	Y	Y	N	Dogger -9.2‰ ±1.3 Malm -8.5‰ ±0.4	Average -8.9‰ ±0.9	-8.9‰ ±1.3	Dull	Y	-9.6‰ ±1

Lu. = Luminescence; Zo. = Zoning; Por. = Porosity filling; Frac. = Fracture filling; Fe = Ferroan; Y = Yes; N = No

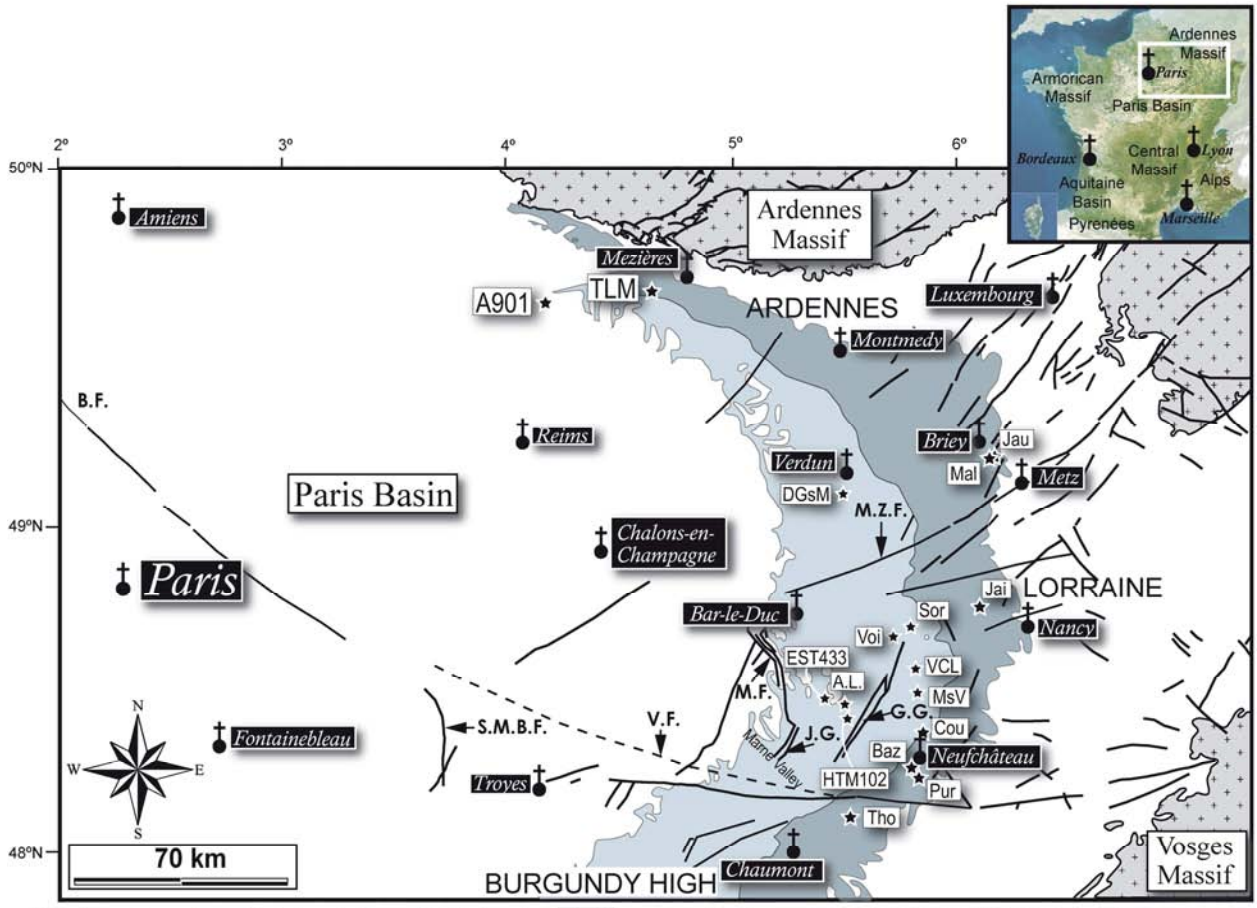

★ Studied sections Late Jurassic Middle Jurassic Basement A.L. = Andra laboratory (EST204, EST205, EST210 cored drills)

B.F. = Bray fault; **S.M.B.F.** = Saint-Martin de Bossenay fault; **V.F.** = Vittel fault; **M.Z.F.** = Metz fault; **M.F.** = Marne faults; **J.G.** = Joinville graben; **G.G.** = Gondrecourt graben

Baz = Bazoilles-sur-Meuse Cou = Coussey DGsM = Dugny-sur-Meuse Jai = Jaillon Jau = Jaumont Mal = Malancourt-la-montagne MsV = Maxey-sur-Vaise

VCL = Vaucouleurs Voi = Void-Vacon Sor = Sorcy Tho = Thol-les-Millières TLM = Thin-le-Moutier Pur = Punerot

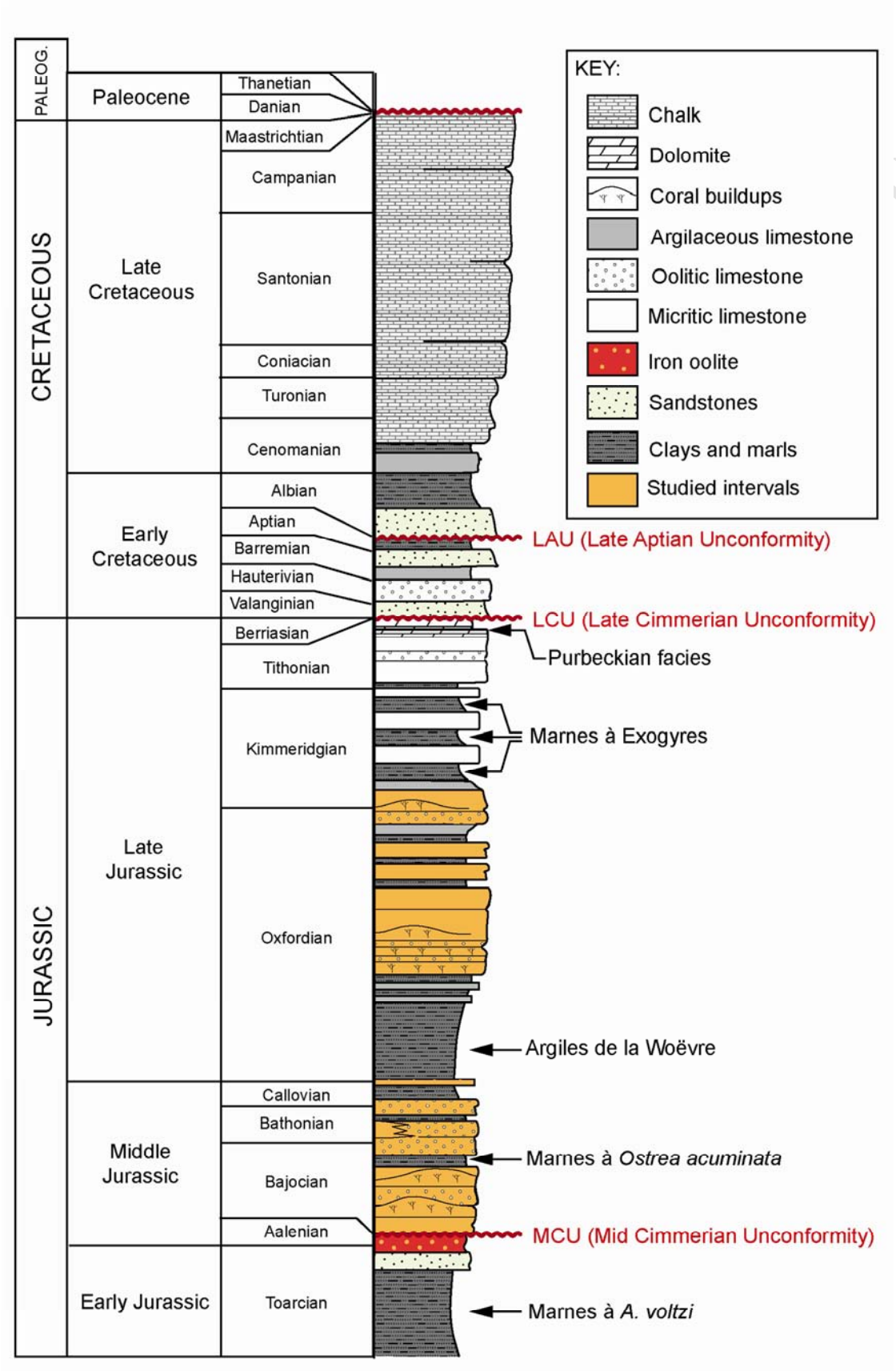
PALEOG.
CRETACEOUS
JURASSIC
Paleocene
Late Cretaceous
Early Cretaceous
Late Jurassic
Middle Jurassic
Early Jurassic
Thanetian
Danian
Maastrichtian
Campanian
Santonian
Coniacian
Turonian
Cenomanian
Albian
Aptian
Barremian
Hauterivian
Valanginian
Berriasian
Tithonian
Kimmeridgian
Oxfordian
Callovian
Bathonian
Bajocian
Aalenian
Toarcian
KEY:
Chalk
Dolomite
Coral buildups
Argilaceous limestone
Oolitic limestone
Micritic limestone
Iron oolite
Sandstones
Clays and marls
Studied intervals
LAU (Late Aptian Unconformity)
LCU (Late Cimmerian Unconformity)
Purbeckian facies
Marnes à Exogyres
Argiles de la Woëvre
Marnes à Ostrea acuminata
MCU (Mid Cimmerian Unconformity)
Marnes à A. voltzi

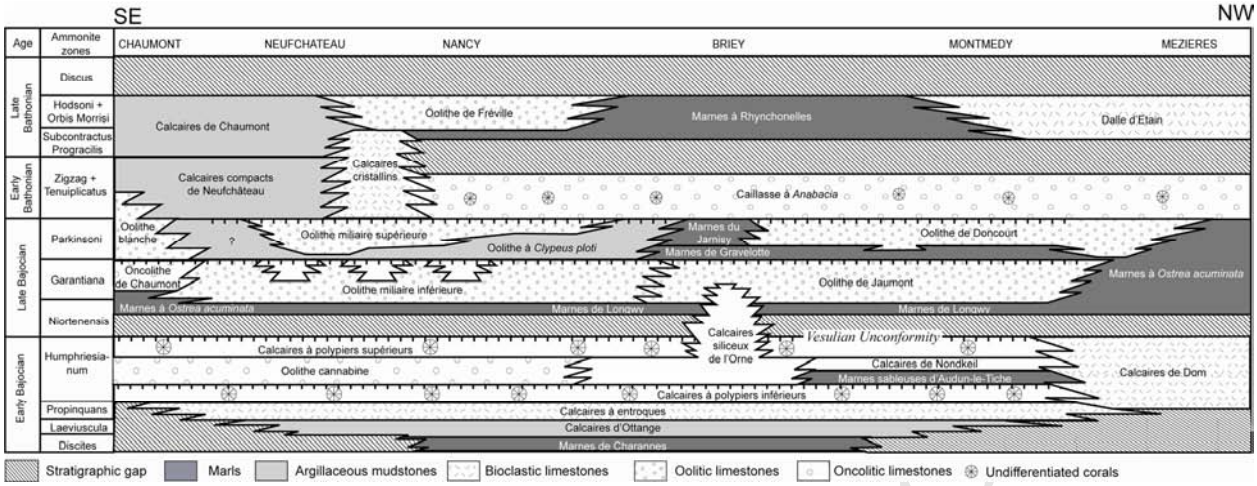

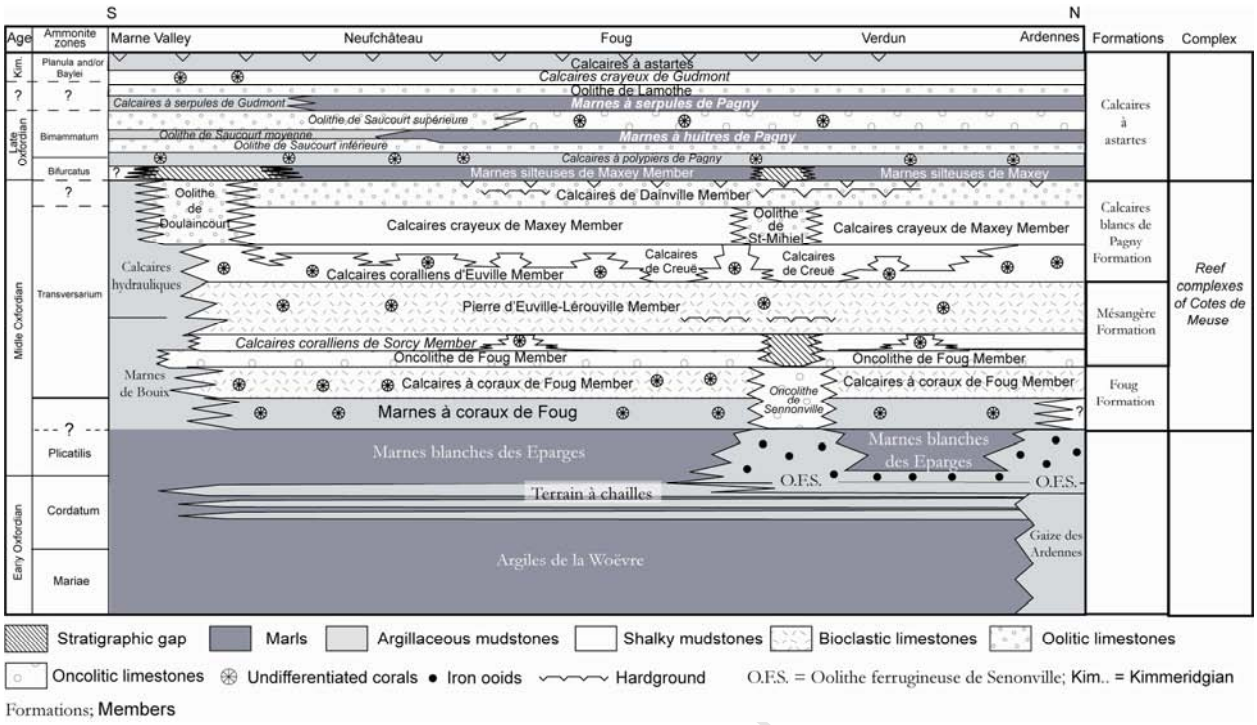

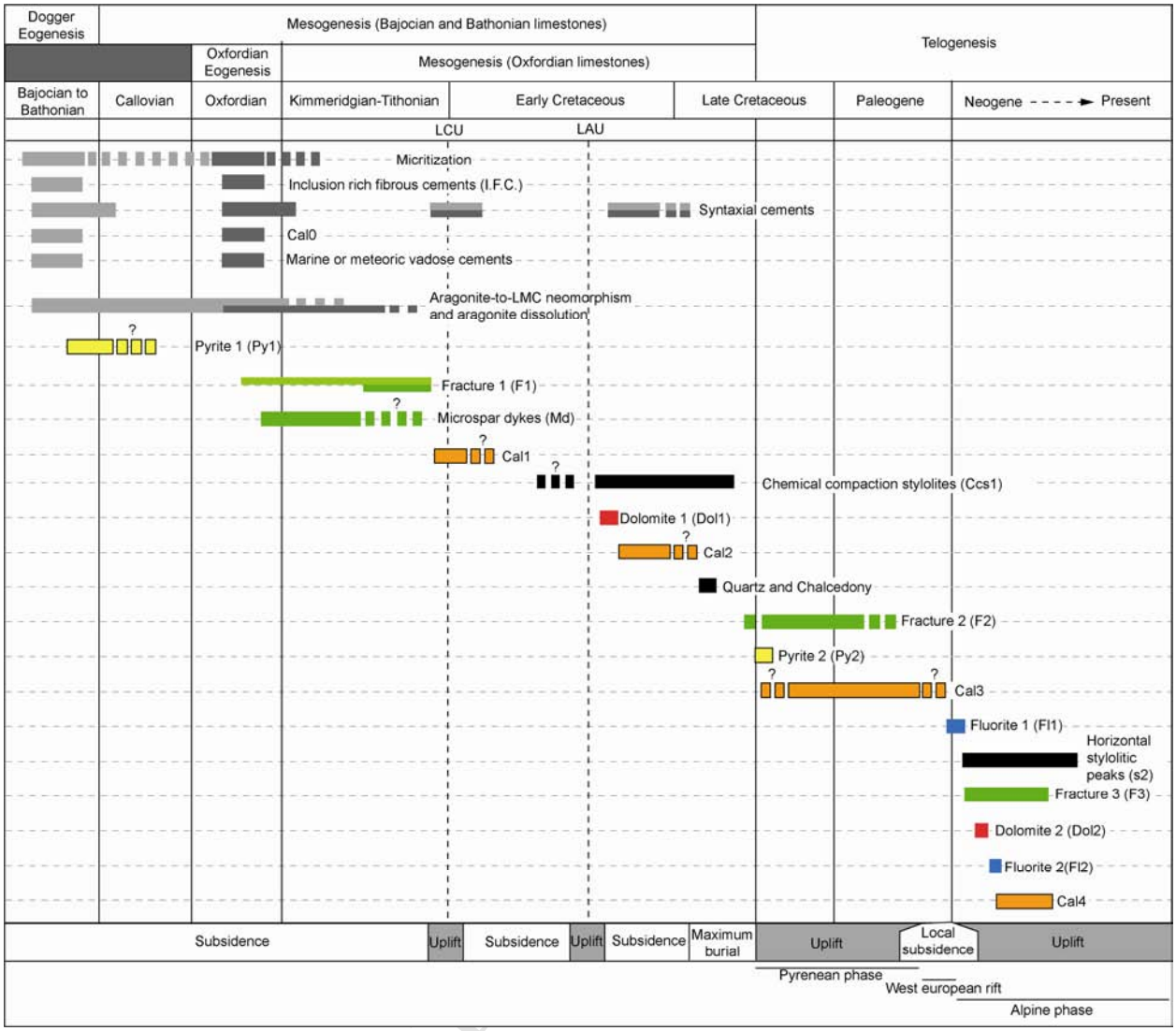
Dogger Eogenesis
Mesogenesis (Bajocian and Bathonian limestones)
Telogenesis
Oxfordian Eogenesis
Mesogenesis (Oxfordian limestones)
Bajocian to Bathonian
Callovian
Oxfordian
Kimmeridgian-Tithonian
Early Cretaceous
Late Cretaceous
Paleogene
Neogene
Present
LCU
LAU
Micritization
Inclusion rich fibrous cements (I.F.C.)
Syntaxial cements
Cal0
Marine or meteoric vadose cements
Aragonite-to-LMC neomorphism and aragonite dissolution
Pyrite 1 (Py1)
Fracture 1 (F1)
Microspar dykes (Md)
Cal1
Chemical compaction stylolites (Ccs1)
Dolomite 1 (Dol1)
Cal2
Quartz and Chalcedony
Fracture 2 (F2)
Pyrite 2 (Py2)
Cal3
Fluorite 1 (Fl1)
Horizontal stylolitic peaks (s2)
Fracture 3 (F3)
Dolomite 2 (Dol2)
Fluorite 2(Fl2)
Cal4
Subsidence
Uplift
Subsidence
Uplift
Subsidence
Maximum burial
Uplift
Local subsidence
Uplift
Pyrenean phase
West european rift
Alpine phase

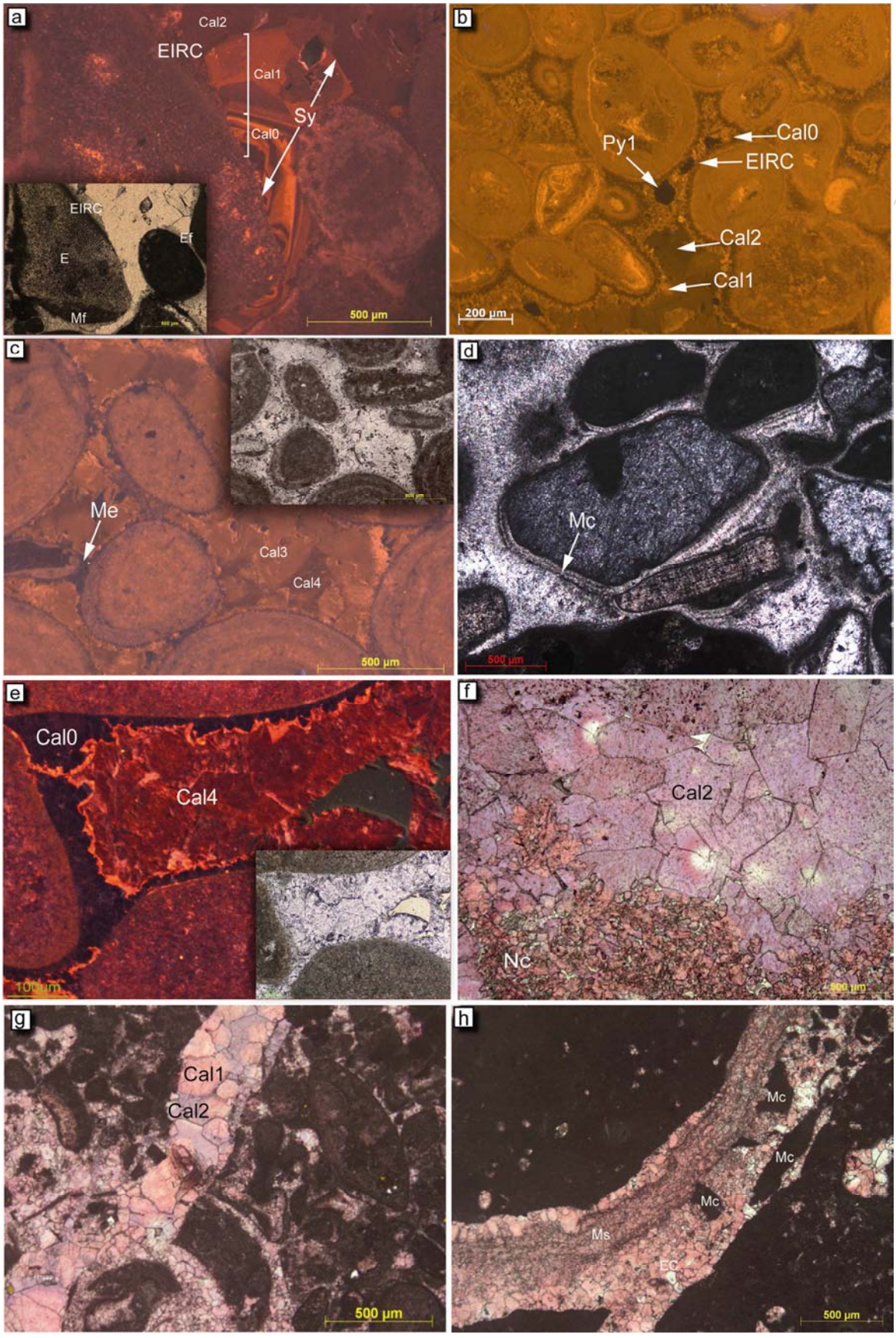
a
Cal2
EIRC
Cal1
Sy
Cal0
EIRC
Ef
E
Mf
500 µm
b
Py1
Cal0
EIRC
Cal2
Cal1
200 µm
c
Me
Cal3
Cal4
500 µm
d
Mc
500 µm
e
Cal0
Cal4
100 µm
f
Cal2
Nc
500 µm
g
Cal1
Cal2
500 µm
h
Mc
Mc
Mc
Ms
EC
500 µm

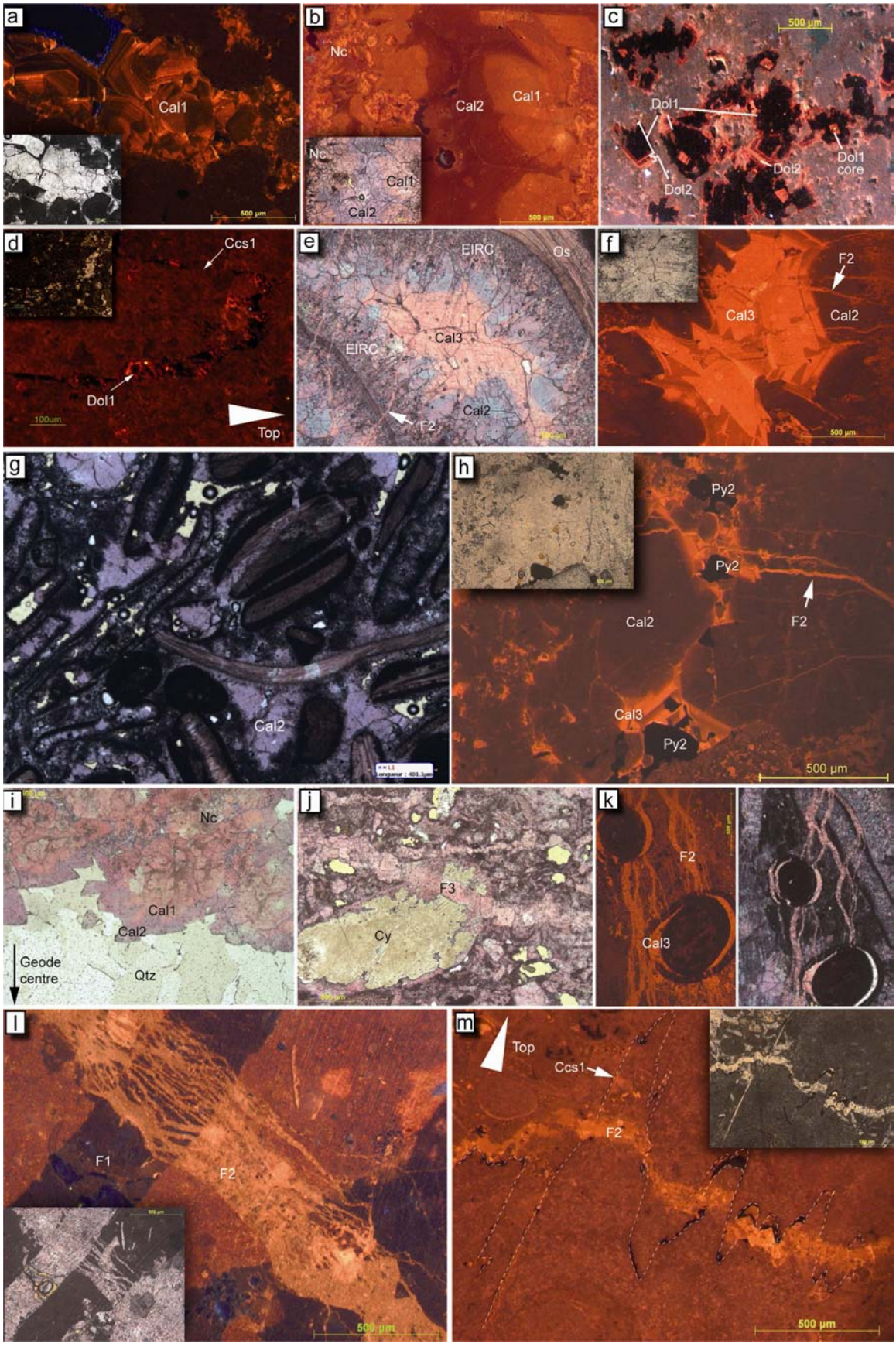
a
Cal1
b
Nc
Cal2
Cal1
Nc
Cal1
Cal2
c
500 µm
Dol1
Dol2
Dol1 core
Dol2
d
Ccs1
Dol1
100um
Top
e
EIRC
Os
Cal3
EIRC
Cal2
F2
f
F2
Cal3
Cal2
500 µm
g
Cal2
h
Py2
Py2
Cal2
F2
Cal3
Py2
500 µm
i
Nc
Cal1
Cal2
Geode centre
Qtz
j
F3
Cy
k
F2
Cal3
l
F1
F2
500 µm
m
Top
Ccs1
F2
500 µm

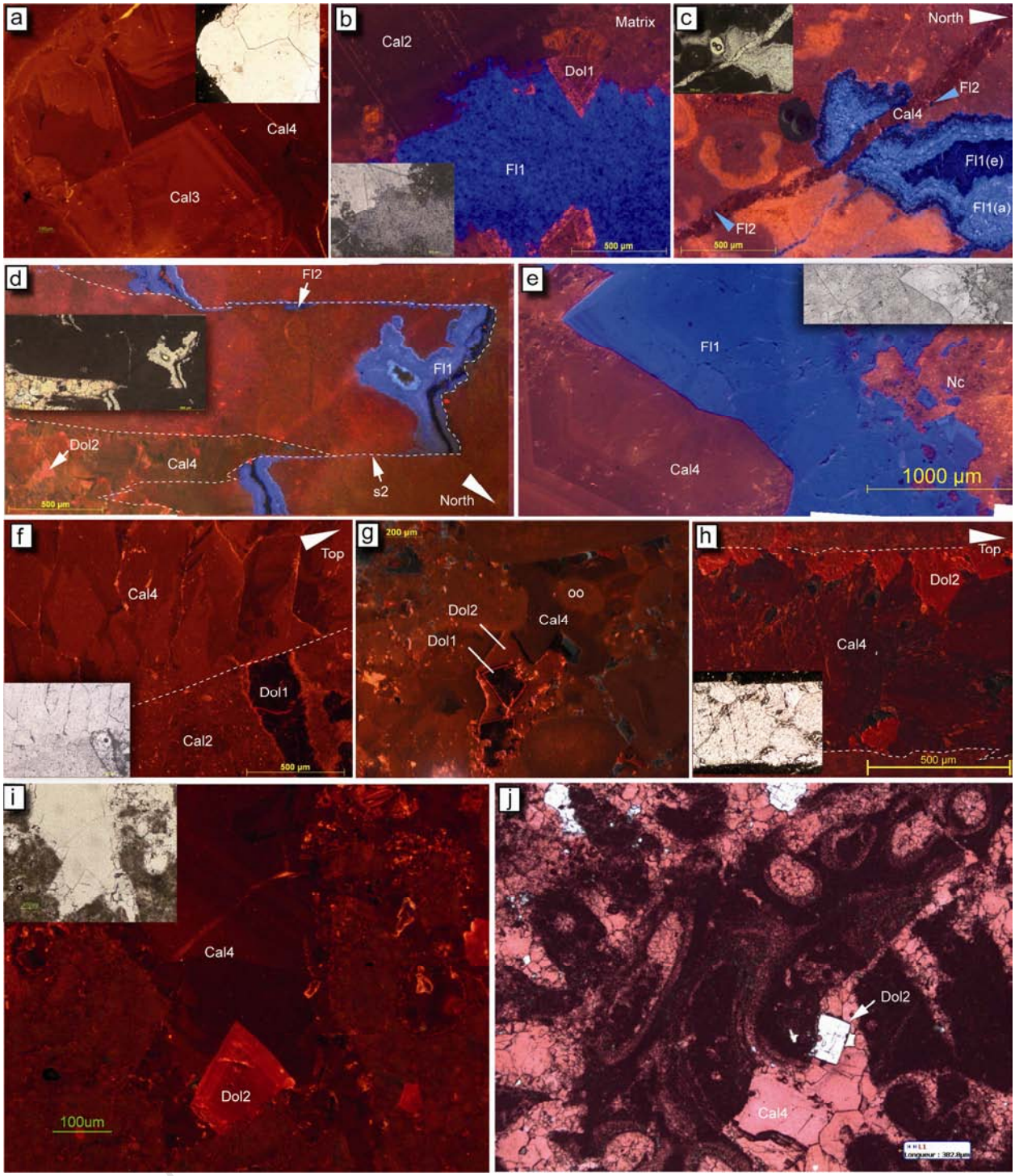
a
Cal4
Cal3
b
Matrix
Cal2
Dol1
Fl1
500 µm
c
North
Fl2
Cal4
Fl1(e)
Fl1(a)
Fl2
500 µm
d
Fl2
Fl1
Dol2
Cal4
s2
North
500 µm
e
Fl1
Nc
Cal4
1000 µm
f
Top
Cal4
Dol1
Cal2
500 µm
g
200 µm
oo
Dol2
Cal4
Dol1
h
Top
Dol2
Cal4
500 µm
i
Cal4
Dol2
100um
j
Dol2
Cal4

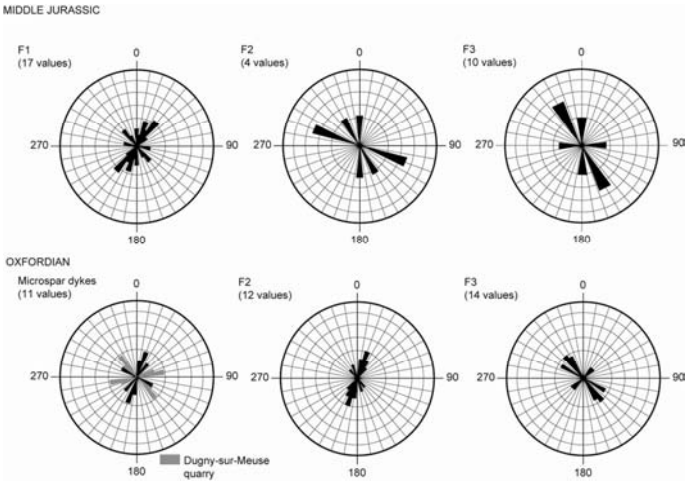

a) Present study

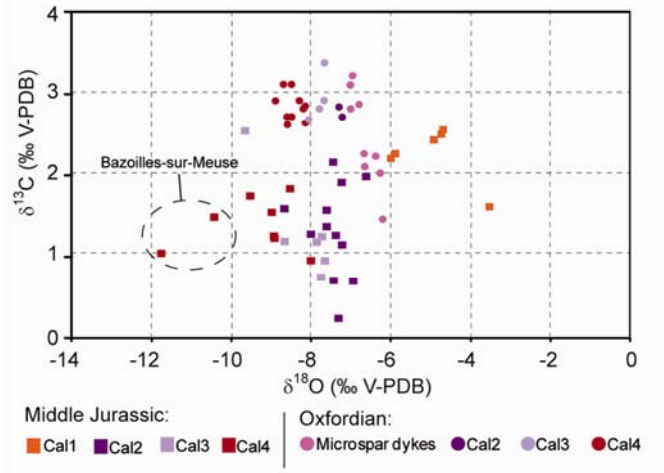

b) Shells, geodes and intergranular porosity cements from the litterature

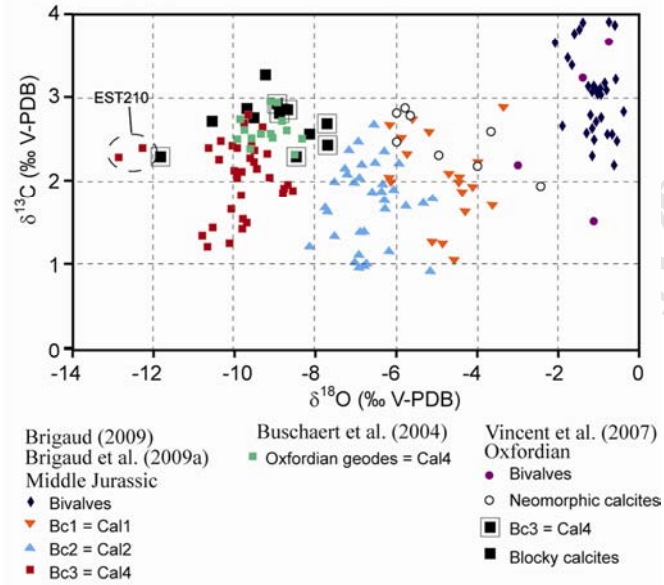

c) Faults and tension gashes calcites from the litterature

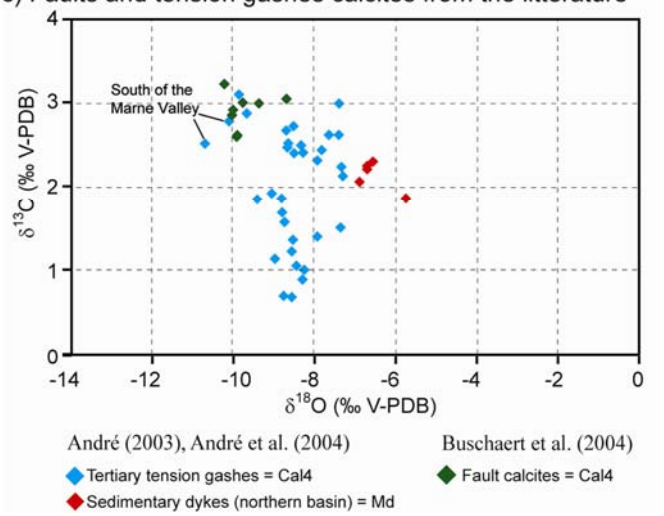

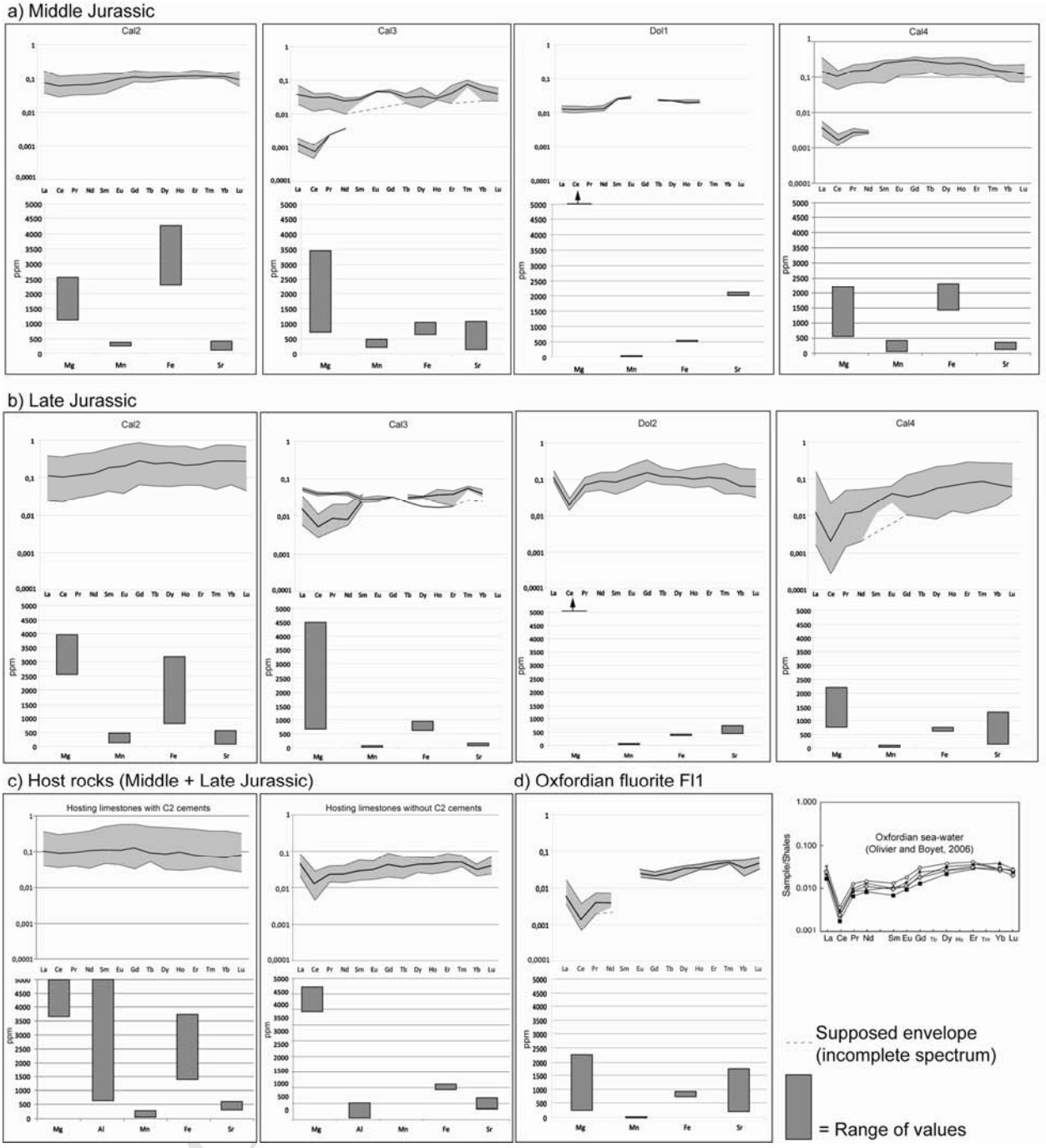
a) Middle Jurassic
Cal2
Cal3
Dol1
Cal4
b) Late Jurassic
Cal2
Cal3
Dol2
Cal4
c) Host rocks (Middle + Late Jurassic)
Hosting limestones with C2 cements
Hosting limestones without C2 cements
d) Oxfordian fluorite FI1
Oxfordian sea-water
(Olivier and Boyet, 2006)
Sample/Shales
Supposed envelope
(incomplete spectrum)
= Range of values
ppm
La Ce Pr Nd Sm Eu Gd Tb Dy Ho Er Tm Yb Lu
Mg Mn Fe Sr
Mg Al Mn Fe Sr

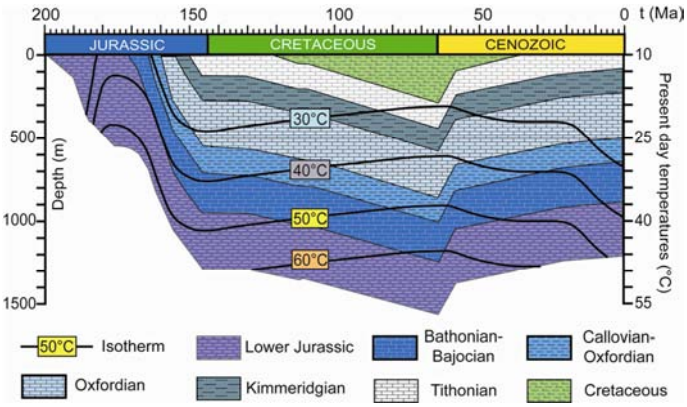

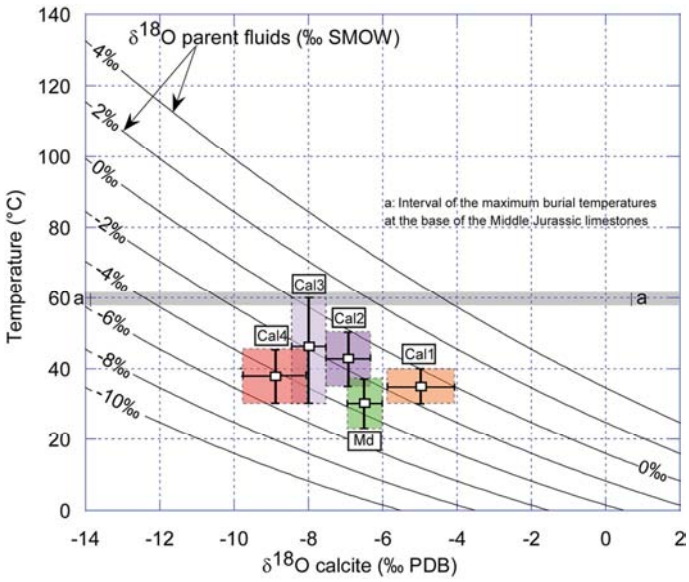

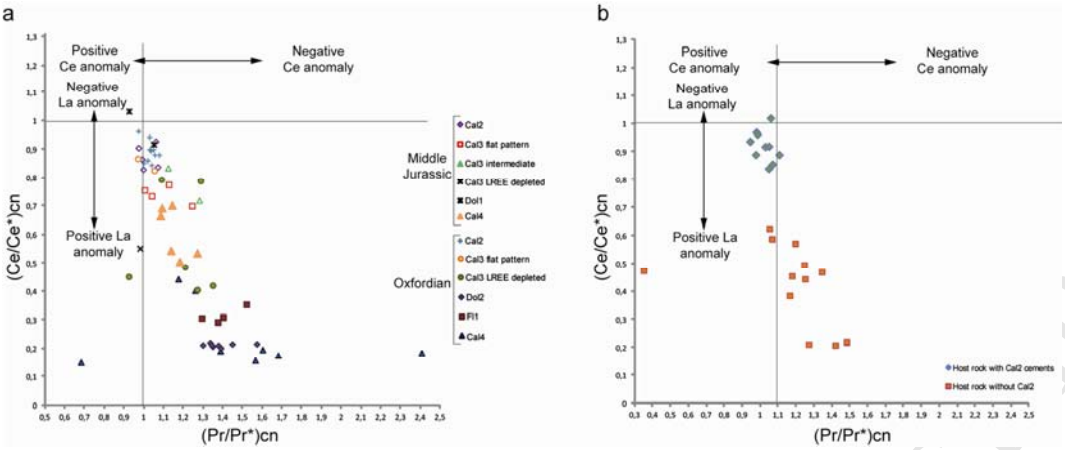

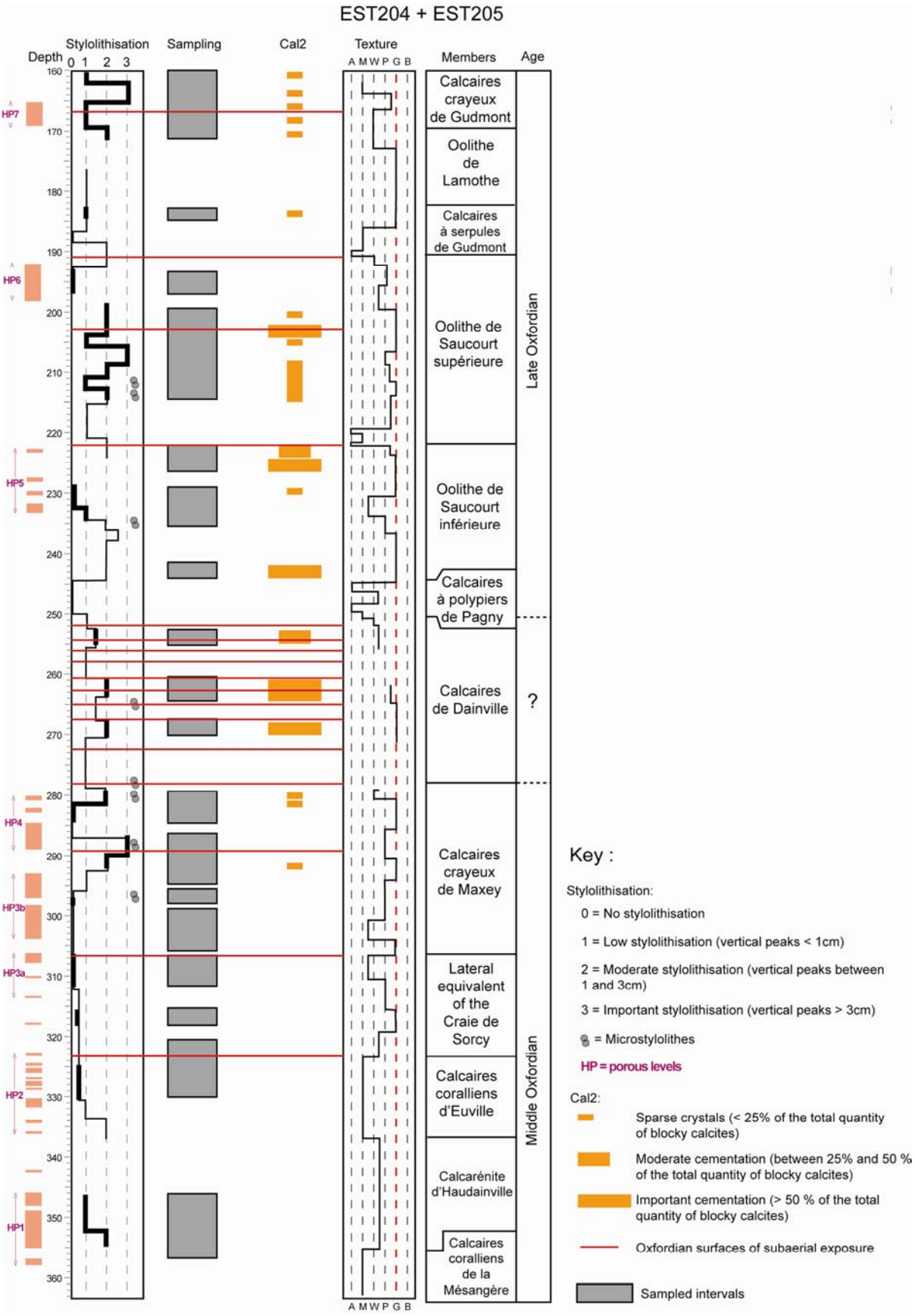
EST204 + EST205
Depth
Stylolithisation
0 1 2 3
Sampling
Cal2
Texture
A M W P G B
Members
Age
Calcaires crayeux de Gudmont
Oolithe de Lamothe
Calcaires à serpules de Gudmont
Oolithe de Saucourt supérieure
Oolithe de Saucourt inférieure
Calcaires à polypiers de Pagny
Calcaires de Dainville
Calcaires crayeux de Maxey
Lateral equivalent of the Craie de Sorcy
Calcaires coralliens d'Euville
Calcarénite d'Haudainville
Calcaires coralliens de la Mésangère
Late Oxfordian
?
Middle Oxfordian
HP7
HP6
HP5
HP4
HP3b
HP3a
HP2
HP1
160
170
180
190
200
210
220
230
240
250
260
270
280
290
300
310
320
330
340
350
360
Key :
Stylolithisation:
0 = No stylolithisation
1 = Low stylolithisation (vertical peaks < 1cm)
2 = Moderate stylolithisation (vertical peaks between 1 and 3cm)
3 = Important stylolithisation (vertical peaks > 3cm)
= Microstylolithes
HP = porous levels
Cal2:
Sparse crystals (< 25% of the total quantity of blocky calcites)
Moderate cementation (between 25% and 50 % of the total quantity of blocky calcites)
Important cementation (> 50 % of the total quantity of blocky calcites)
Oxfordian surfaces of subaerial exposure
Sampled intervals

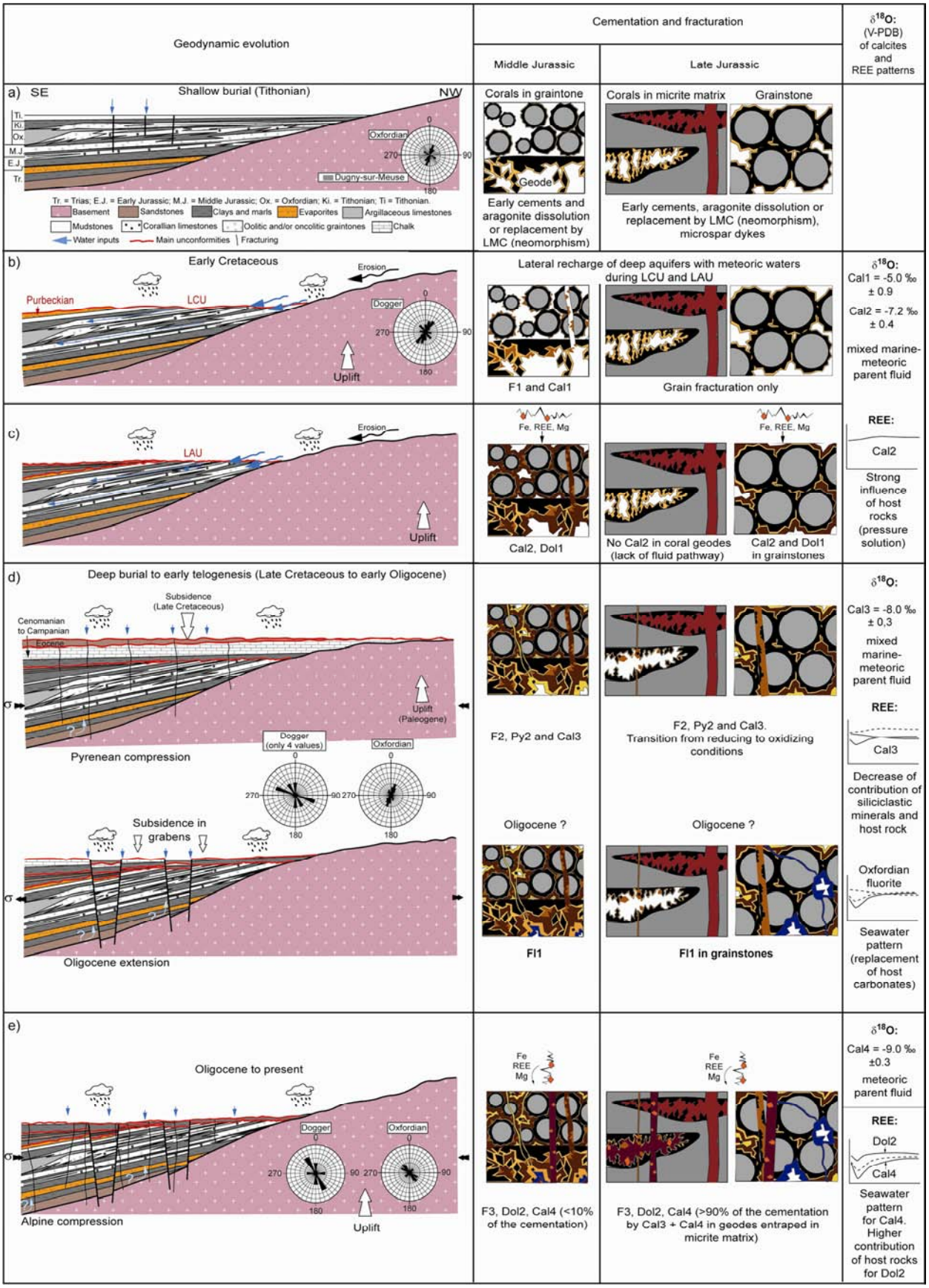
Geodynamic evolution
Cementation and fracturation
Middle Jurassic
Late Jurassic
δ18O: (V-PDB) of calcites and REE patterns
a) SE
Shallow burial (Tithonian)
NW
Ti.
Ki.
Ox.
M.J.
E.J.
Tr.
Oxfordian
Dugny-sur-Meuse
Tr. = Trias; E.J. = Early Jurassic; M.J. = Middle Jurassic; Ox. = Oxfordian; Ki. = Tithonian; Ti = Tithonian.
Basement
Sandstones
Clays and marls
Evaporites
Argillaceous limestones
Mudstones
Corallian limestones
Oolitic and/or oncolitic graintones
Chalk
Water inputs
Main unconformities
Fracturing
Corals in graintone
Geode
Early cements and aragonite dissolution or replacement by LMC (neomorphism)
Corals in micrite matrix
Grainstone
Early cements, aragonite dissolution or replacement by LMC (neomorphism), microspar dykes
b)
Early Cretaceous
Erosion
Purbeckian
LCU
Dogger
Uplift
Lateral recharge of deep aquifers with meteoric waters during LCU and LAU
F1 and Cal1
Grain fracturation only
δ18O:
Cal1 = -5.0 ‰ ± 0.9
Cal2 = -7.2 ‰ ± 0.4
mixed marine-meteoric parent fluid
c)
LAU
Fe, REE, Mg
Cal2, Dol1
No Cal2 in coral geodes (lack of fluid pathway)
Cal2 and Dol1 in grainstones
REE:
Cal2
Strong influence of host rocks (pressure solution)
d)
Deep burial to early telogenesis (Late Cretaceous to early Oligocene)
Subsidence (Late Cretaceous)
Cenomanian to Campanian
Eocene
Uplift (Paleogene)
Pyrenean compression
Dogger (only 4 values)
Oxfordian
Subsidence in grabens
Oligocene extension
F2, Py2 and Cal3
F2, Py2 and Cal3. Transition from reducing to oxidizing conditions
Oligocene ?
FI1
FI1 in grainstones
δ18O:
Cal3 = -8.0 ‰ ± 0,3
mixed marine-meteoric parent fluid
REE:
Cal3
Decrease of contribution of siliciclastic minerals and host rock
Oxfordian fluorite
Seawater pattern (replacement of host carbonates)
e)
Oligocene to present
Alpine compression
Fe
REE
Mg
F3, Dol2, Cal4 (<10% of the cementation)
F3, Dol2, Cal4 (>90% of the cementation by Cal3 + Cal4 in geodes entraped in micrite matrix)
δ18O:
Cal4 = -9.0 ‰ ±0.3
meteoric parent fluid
REE:
Dol2
Cal4
Seawater pattern for Cal4. Higher contribution of host rocks for Dol2

Highlights

- Impact of basin geodynamic on Jurassic carbonate diagenesis of the Paris Basin
- Contribution of calcite REE analysis in the understanding of carbonate diagenesis
- Synthesis of published data and proposal of a new common paragenetic scheme
- Impact of sedimentary facies on the lateral recharge of deep carbonate aquifers

Middle Jurassic

Stratigraphy	Location	Sampling	Calcite	$\delta^{18}O$ ‰(V-PDB)	$\delta^{13}C$ ‰(V-PDB)
Bajocian	Thin le Moutier	Intergranular porosity	Cal1	-6,01	2,18
Bajocian	Thin-le-Moutier	Fracture	Cal1	-5,90	2,24
Bajocian	Thin le Moutier	Geode	Cal1	-4,93	2,41
Bajocian	Thin-le-Moutier	Fracture	Cal1	-4,74	2,48
Bajocian	Thin le Moutier	Geode	Cal1	-4,71	2,53
Bajocian	Thin-le-Moutier	Fracture	Cal1	-3,54	1,58
Bajocian	Jaumont	Fracture	Cal2	-7,24	1,88
Bajocian	Malancourt	Geode	Cal2	-7,44	0,66
Bajocian	Jaillon	Fracture	Cal2	-8,02	1,47
Bajocian	Forage A901	Fracture	Cal2	-7,62	1,24
Bajocian	Jaumont	Fracture	Cal2	-7,23	1,33
Bajocian	Jaumont	Fracture	Cal2	-6,63	1,10
Bajocian	Jaumont	Géode	Cal2	-7,39	1,22
Bajocian	Jaumont	Géode	Cal2	-7,32	0,19
Bajocian	Jaumont	Fracture	Cal2	-7,08	1,95
Late Bathonian	A901 drill core	Fracture	Cal2	-6,66	1,54
Bajocian	Malancourt	Geode	Cal2	-7,46	2,13
Bajocian	Bazoilles-sur-Meuse	Fracture	Cal2	-9,72	1,62
Bajocian	A901 drill core	Fracture	Cal3	-7,74	1,21
Late Bathonian	A901 drill core	Geode	Cal3	-8,67	1,15
Late Bathonian	A901 drill core	Geode	Cal3	-7,87	1,14
Bajocian	Thol-les-Millières	Fracture	Cal3	-9,65	2,52
Middle Bathonian	A901 drill core	Intergranular porosity	Cal3	-7,76	0,70
Late Bathonian	A901 drill core	Fracture	Cal3	-7,68	0,91
Bajocian	Bazoilles-sur-Meuse	Fracture	Cal4	-11,77	1,00
Bajocian	Bazoilles-sur-Meuse	Fracture	Cal4	-10,44	1,45
Bajocian	A901 drill core	Fracture	Cal4	-8,94	1,21
Bajocian	A901 drill core	Fracture	Cal4	-8,94	1,19
Early Bathonian	A901 drill core	Fracture	Cal4	-8,54	1,80
Middle Bathonian	Coussey	Geode	Cal4	-8,68	1,55
Late Bathonian	A901 drill core	Intergranular porosity	Cal4	-8,02	0,91
Bajocian	Punerot	Fracture	Cal4	-8,96	1,47
Bajocian	Punerot	Fracture	Cal4	-9,46	1,73

Late Jurassic

Stratigraphy	Location	Sampling	Calcite	$\delta^{18}O$ ‰(V-PDB)	$\delta^{13}C$ ‰(V-PDB)
Late Oxfordian	EST205 drill core	Geode	Cal3	-7,80	2,80
Middle Oxfordian	EST204 drill core	Fracture	Cal4	-8,50	3,10
Middle Oxfordian	EST204 drill core	Intergranular porosity	Cal4	-8,70	3,10
Middle Oxfordian	EST204 drill core	Geode	Cal4	-8,30	2,90
Middle Oxfordian	EST205 drill core	Geode	Cal4	-8,30	2,90
Middle Oxfordian	EST205 drill core	Geode	Cal4	-8,60	2,70
Middle Oxfordian	EST205 drill core	Geode	Cal4	-8,90	2,90
Middle Oxfordian	EST205 drill core	Geode	Cal4	-8,20	2,80
Middle Oxfordian	EST205 drill core	Fracture	Cal4	-8,50	2,70
Middle Oxfordian	EST204 drill core	Intergranular porosity	Cal4	-8,60	2,60
Late Oxfordian	EST204 drill core	Geode	Cal4	-8,15	2,62
Late Oxfordian	EST204 drill core	Geode	Cal4	-8,16	2,83
Late Oxfordian	EST204 drill core	Geode	Cal3	-8,07	2,66
Middle Oxfordian	Maxey-sur-Vaise	Fracture	Cal3	-7,69	2,90
Middle Oxfordian	Vaucouleurs	Fracture	Cal3	-7,68	3,37
Middle Oxfordian	Dugny-sur-Meuse	Geode	Md1	-6,39	2,20
Middle Oxfordian	Dugny-sur-Meuse	Geode	Md1	-6,81	2,85
Middle Oxfordian	Dugny-sur-Meuse	Geode	Md1	-6,68	2,23
Middle Oxfordian	Dugny-sur-Meuse	Geode	Md1	-6,67	2,08
Middle Oxfordian	Dugny-sur-Meuse	Geode	Md1	-6,28	1,99
Middle Oxfordian	Sorcy	Geode	Md1	-6,22	1,42
Middle Oxfordian	Void-Vacon	Fracture	Md1	-7,03	3,09
Middle Oxfordian	Sorcy	Geode	Md1	-7,02	2,80
Middle Oxfordian	Sorcy	Fracture	Md1	-6,98	3,21
Late Oxfordian	A901 drill core	Fracture	Cal2	-7,31	2,82
Late Oxfordian	A901 drill core	Geode	Cal2	-7,23	2,70